

# PERIPHERAL NUCLEON–NUCLEON PHASE SHIFTS AND CHIRAL SYMMETRY\*

N. Kaiser<sup>a</sup>, R. Brockmann<sup>b</sup> and W. Weise<sup>a</sup>

<sup>a</sup> *Physik Department, Technische Universität München,  
D-85747 Garching, Germany*

<sup>b</sup> *Institut für Kernphysik, Universität Mainz, D-55099 Mainz, Germany*

## Abstract

Within the one-loop approximation of baryon chiral perturbation theory we calculate all one-pion and two-pion exchange contributions to the nucleon-nucleon interaction. In fact we construct the elastic NN-scattering amplitude up to and including third order in small momenta. The phase shifts with orbital angular momentum  $L \geq 2$  and the mixing angles with  $J \geq 2$  are given parameterfree and thus allow for a detailed test of chiral symmetry in the two-nucleon system. We find that for the D-waves the  $2\pi$ -exchange corrections are too large as compared with empirical phase shifts, signaling the increasing importance of shorter range effects in lower partial waves. For higher partial waves, especially for G-waves, the model independent  $2\pi$ -exchange corrections bring the chiral prediction close to empirical NN phase shifts. We propose to use the chiral NN phase shifts with  $L \geq 3$  as input in a future phase shift analysis. Furthermore, we compute the irreducible two-pion exchange NN-potentials in coordinate space. They turn out to be of van-der-Waals type, with exponential screening of two-pion mass range.

---

\*Work supported in part by BMBF and DFG.

## I. INTRODUCTION

The force between two nucleons is one of the fundamental problems in nuclear physics. Experimentally, the two-nucleon force is mapped out in nucleon-nucleon scattering, which is a purely elastic process up to nucleon laboratory kinetic energies of  $T_{lab} = 280$  MeV, the  $NN\pi^0$ -threshold. Since both the target and the projectile have spin-1/2, there is a rich spin-structure in NN-scattering. Besides total and differential cross sections many independent spin-observables can be measured with polarized targets and/or projectiles. At present a huge body of NN-scattering data exists and this data base will increase and improve in the near future, in particular with experiments to be performed at the proton cooler facility COSY in Jülich.

The theoretical interpretation of the elastic NN-scattering data is done in terms of a phase shift analysis. The pertinent phase shifts are labeled by the spectroscopic notation  $^{2S+1}L_J$ , with  $S = 0, 1$  the total spin,  $J = 0, 1, 2, \dots$  the total angular momentum and  $L = J - S, J, J + S$  the orbital angular momentum of the two-nucleon system. The total isospin of the NN-system  $I = 0, 1$  is readily determined by the Pauli exclusion principle, which demands  $I + S + L$  to be odd, in order to have an antisymmetric wave function in the combined isospin-spin-coordinate space. The spin-dependence of one-pion exchange (longest range NN-interaction) gives rise to a tensor interaction which causes a mixing of the (triplet) states with orbital angular momentum  $L = J - 1$  and  $L = J + 1$ . In order to quantify this effect a mixing angle  $\epsilon_J$  is introduced for each  $J$  in addition to the singlet and the three triplet phase shifts. The empirical mixing angles  $\epsilon_J$  are, however, small and do not exceed 7 degrees up to the  $NN\pi^0$ -threshold. This weak mixing justifies the use of the spectroscopic notation  $^{2S+1}L_J$  which presumes  $L$  to be a good quantum number.

The single (weakly) bound state, the deuteron in the  $^3S_1$ -channel with total isospin  $I = 0$ , shows up as a pole in the NN-scattering amplitude (on the physical Riemann-sheet of  $T_{lab}$ ) slightly below threshold at  $T_{lab} = -4.45$  MeV, corresponding to minus twice the deuteron binding energy [1]. In the  $^1S_0$ -channel with total isospin  $I = 1$  the nucleon-nucleon potential is slightly too weak to form a bound state and a pole on the second Riemann-sheet results [2], even much closer to threshold than the deuteron pole. Both the true bound state deuteron and the "anti-bound" state on the second Riemann-sheet slightly below threshold are responsible for the extraordinarily large S-wave NN-scattering lengths [3] ( $a(^3S_1) = -5.42$  fm,  $a(^1S_0) = 23.75$  fm) and the rapid change of the S-wave phase shifts. In all other partial waves the energy dependence is much more moderate. P- and D-wave phase shifts change by at most  $30^\circ$  from threshold up to the  $NN\pi^0$ -threshold at  $T_{lab} = 280$  MeV and F- and G-waves do not exceed values of  $7^\circ$  in this energy range [4]. Thus with the exception of the two S-waves, the nucleon-nucleon interaction is actually rather weak in almost all channels.

An accurate description of the NN-scattering data and deuteron properties has been found in terms of the one-boson-exchange model (OBE) and more refined the Bonn-potential [5] which includes multi-meson exchanges as well. The basic ingredients of the OBE model are the one-pion exchange, the exchange of the vector mesons  $\rho(770)$  and  $\omega(782)$ , and the exchange of a fictitious scalar isoscalar boson  $\sigma(550)$ . The latter may be viewed as an effective description of correlated two-pion exchange in the isoscalar scalar channel. Such an interpretation of the  $\sigma(550)$  comes from the dispersion-theoretical studies of the two-pion exchange [6], which use the empirical information from the crossed  $\pi N$ -scattering channel. The coupling constants of the vector and scalar mesons to the

nucleon are adjustable parameters. For each meson-nucleon vertex a "form factor" of monopole-type with adjustable cut-off in the range  $1 \text{ GeV} < \Lambda < 2 \text{ GeV}$  is introduced. In the OBE model these form factors are needed to have convergent integrals in the Lippmann-Schwinger equation, which iterates the OBE potential to infinite orders. Even though the meson-nucleon form factors are often interpreted (in analogy with the electromagnetic nucleon form factors) in terms of nucleon substructure, they do not represent truly physical quantities. First, they cannot be measured, and secondly they cannot even be defined in a model independent way. As off-shell matrix elements they depend on the actual form of the interpolating meson field, which is not unique for a composite particle. Putting aside the non-observability of meson-nucleon form factors, the OBE-model works very well. With about a dozen free parameters one obtains accurate fits to NN-scattering data and deuteron properties [5].

In recent years there has been activity to understand the NN-force in a more fundamental way from the symmetries of QCD, in particular from chiral symmetry which governs low-energy strong interactions. In his seminal papers Weinberg [7] discussed the qualitative implications of chiral symmetry for the two- and multi-nucleon forces. Ordonez, Ray and van Kolck [8] applied the chiral Lagrangian to the two-nucleon problem. Using time-ordered perturbation theory and a Gaussian cut-off prescription to regularize loop divergences they calculated the two-pion exchange NN-potential. In addition more than 20 parameters related to short range NN-contact terms were introduced. The cut-off dependent potential was then transformed to coordinate space and used to solve the non-relativistic Schrödinger equation. A good fit was obtained for the deuteron properties and the phase shifts in the low partial waves (S, P, D) up to kinetic energies of  $T_{lab} = 100 \text{ MeV}$  (partly also up to  $T_{lab} = 300 \text{ MeV}$ ) [8]. Of course in the presence of nearly 30 fit parameters the role of chiral symmetry in the NN-interaction is obscured. Furthermore, the use of a Gaussian cut-off is not consistent with the chiral power counting scheme underlying the whole approach [7].

The purpose of this work is to explore the kinematical window in energy and angular momentum in which the NN-interaction is governed by chiral symmetry alone. Our physical motivation comes from the simple fact that the range of the force produced by the exchange of a hadronic state is inversely proportional to its mass. The longest range part comes from one-pion exchange and chiral symmetry manifests itself via the smallness of the pion mass, a feature which derives from the fact that the pion is an approximate Goldstone boson of spontaneous chiral symmetry breaking in QCD. The exchange of the next heavier hadronic state, consisting of two pions, is intimately related to  $\pi N$ -scattering by crossing. In this reaction chiral symmetry leads to important dynamical constraints in the form of low-energy theorems [9], see also the recent work of [10], where many low-energy  $\pi N$ -observables have been investigated in chiral perturbation theory. It is now interesting to explore the structure of the  $2\pi$ -exchange NN-potential when it is produced by a  $\pi N$ -interaction with all chiral constraints built in. Naturally, one expects such an approach to work for the peripheral NN-partial waves where only the long and intermediate range components of the NN-force operate.

In the present work we calculate the chiral two-pion exchange based on the same chiral  $\pi N$ -Lagrangian as used in [8]. Our methods and aims are however different and complementary. First of all we will use covariant perturbation theory throughout and thus have to solve the problem of the so-called pinch singularity [7] occurring in the planar box diagram. Secondly, we use throughout dimensional regularization, a prescription to

handle loop divergences which is in harmony with chiral symmetry and the chiral power counting scheme. Thirdly, we stay within the systematic expansion of chiral perturbation theory and calculate in one-loop approximation all contributions to the NN T-matrix up to and including third order in small external momenta. Consequently, we do not iterate to infinite orders. As a result we find that the phase shifts with  $L \geq 2$  and mixing angles with  $J \geq 2$  are given entirely parameterfree and thus allow for a rigorous test of chiral symmetry in the NN-interaction.

The paper is organized as follows. In section 2, we briefly discuss the chiral  $\pi N$ -Lagrangian at next-to-leading order underlying our calculation. In section 3, we introduce the necessary formalism, the nucleon-nucleon T-matrix, the projection onto partial waves and the expressions for the perturbative phase-shifts and mixing angles. Section 4 presents closed form analytical results for the one-pion and two-pion exchange contributions to the NN T-matrix calculated in one-loop approximation. In section 5 the parameterfree results for the peripheral phase shifts ( $L \geq 2$ ) and mixing angles ( $J \geq 2$ ) are discussed. In section 6 we give explicit expressions for the irreducible two-pion exchange potentials in coordinate space and compare them with phenomenological ones. In section 7 we compare the isoscalar central amplitude at zero momentum transfer with OBE and finally section 8 ends with a summary. In the appendix the construction of the anti-symmetric NN T-matrix satisfying the Pauli exclusion principle is given.

## II. EFFECTIVE CHIRAL LAGRANGIAN

The tool to investigate the dynamical consequences of spontaneous and explicit chiral symmetry breaking in QCD is the effective chiral Lagrangian. It provides a non-linear realization of the chiral symmetry group  $SU(2)_L \times SU(2)_R$  using the relevant low-energy effective degrees of freedom, the Goldstone pions and the nucleons. The effective chiral  $\pi N$ -Lagrangian takes the following general form,

$$\mathcal{L} = \mathcal{L}_{\pi N}^{(1)} + \mathcal{L}_{\pi N}^{(2)} + \dots \quad (1)$$

where the superscript indicates the number of derivatives or small external momenta. In the heavy baryon formulation [11] (which essentially corresponds to a non-relativistic treatment of the nucleons) the leading and next-to-leading order terms read [10,12],

$$\begin{aligned} \mathcal{L}_{\pi N}^{(1)} &= \bar{N} \left( iD_0 - \frac{g_A}{2} \vec{\sigma} \cdot \vec{u} \right) N, \\ \mathcal{L}_{\pi N}^{(2)} &= \bar{N} \left( \frac{1}{2M} \vec{D} \cdot \vec{D} + i \frac{g_A}{4M} \{ \vec{\sigma} \cdot \vec{D}, u_0 \} + 2c_1 m_\pi^2 (U + U^\dagger) \right. \\ &\quad \left. + \left( c_2 - \frac{g_A^2}{8M} \right) u_0^2 + c_3 u_\mu u^\mu + \frac{i}{2} \left( c_4 + \frac{1}{4M} \right) \vec{\sigma} \cdot (\vec{u} \times \vec{u}) \right) N. \end{aligned} \quad (2)$$

Here,  $D^\mu = \partial^\mu + \frac{1}{2}[\xi^\dagger, \partial^\mu \xi]$  is the chiral covariant derivative acting on the iso-doublet nucleon field  $N$  and  $u^\mu = i\{\xi^\dagger, \partial^\mu \xi\}$  is an axial vector (matrix) quantity. The  $SU(2)$ -matrix  $U = \xi^2$  collects the Goldstone pion fields in the form  $U = 1 + i\vec{\tau} \cdot \vec{\pi}/f_\pi - \vec{\pi}^2/2f_\pi^2 + \dots$  with the pion decay constant  $f_\pi = 92.4$  MeV. The only other parameter occurring in  $\mathcal{L}_{\pi N}^{(1)}$  is  $g_A$ , the axial vector coupling constant of the nucleon. Since we are considering here exclusively the pion-nucleon vertex we employ the Goldberger-Treiman relation  $g_A =$

$g_{\pi N} f_{\pi}/M$  together with the empirical value of  $g_{\pi N} = 13.4$  [13] and therefore use  $g_A = 1.32$  throughout.  $M = 939$  MeV is the (average) nucleon mass and  $m_{\pi} = 138$  MeV the (average) pion mass.

The second order Lagrangian  $\mathcal{L}_{\pi N}^{(2)}$  consists of two different types of terms. The first two terms in eq.(3) have coefficients  $1/2M$  and  $g_A/4M$  which are fixed by Lorentz invariance [11]. The remaining set of chiral invariant terms are accompanied by new low-energy constants  $c_1, c_2, c_3, c_4$ . These four low-energy constants have been recently determined at one-loop order in ref. [10] from a fit to nine (sub)threshold  $\pi N$ -observables. Their values are  $c_1 = -0.9 \pm 0.1$ ,  $c_2 = 3.3 \pm 0.2$ ,  $c_3 = -5.3 \pm 0.2$ ,  $c_4 = 3.6 \pm 0.1$ , all given in  $\text{GeV}^{-1}$ . As shown in ref. [10] the  $\Delta(1232)$ -resonance makes the dominant contribution to  $c_2, c_3$  and  $c_4$ . The exchange of a scalar boson with mass and coupling constant similar to the fictitious  $\sigma(550)$  allows to explain  $c_1$  and also part of  $c_3$ . Furthermore,  $c_4$  receives a significant contribution from  $\rho(770)$  vector meson exchange. Note that the  $c_i$  are much larger than the typical  $1/2M$ -scale in eq.(3). Thus one expects the important  $2\pi$ -exchange contributions to the NN T-matrix to be the ones proportional to  $c_i$ . This completes the description of the effective chiral  $\pi N$ -Lagrangian.

### III. FORMALISM

We are considering elastic nucleon-nucleon scattering  $N(\vec{p}) + N(-\vec{p}) \rightarrow N(\vec{p}') + N(-\vec{p}')$ , where  $\pm\vec{p}$  and  $\pm\vec{p}'$  are the initial and final nucleon momenta in the center-of-mass (CM) frame with  $p = |\vec{p}| = |\vec{p}'|$ . The momentum transfer  $\vec{q} = \vec{p}' - \vec{p}$  has the magnitude  $q = |\vec{q}| = 2p \sin \frac{\theta}{2} = p\sqrt{2(1-z)}$ . Here  $\theta$  is the CM scattering angle with  $z = \cos \theta$ . In terms of the nucleon laboratory kinetic energy  $T_{lab}$ , the CM momentum  $p$  is given as  $p = \sqrt{T_{lab}M/2}$ .

In the center-of-mass frame the elastic on-shell nucleon-nucleon T-matrix takes the following general form,

$$\begin{aligned} \mathcal{T}_{NN} = & V_C + \vec{\tau}_1 \cdot \vec{\tau}_2 W_C + [V_S + \vec{\tau}_1 \cdot \vec{\tau}_2 W_S] \vec{\sigma}_1 \cdot \vec{\sigma}_2 + [V_T + \vec{\tau}_1 \cdot \vec{\tau}_2 W_T] \vec{\sigma}_1 \cdot \vec{q} \vec{\sigma}_2 \cdot \vec{q} + \\ & [V_{SO} + \vec{\tau}_1 \cdot \vec{\tau}_2 W_{SO}] i(\vec{\sigma}_1 + \vec{\sigma}_2) \cdot (\vec{q} \times \vec{p}) + [V_Q + \vec{\tau}_1 \cdot \vec{\tau}_2 W_Q] \vec{\sigma}_1 \cdot (\vec{q} \times \vec{p}) \vec{\sigma}_2 \cdot (\vec{q} \times \vec{p}) \end{aligned} \quad (4)$$

with the ten complex functions  $V_C(p, z), \dots, W_Q(p, z)$  depending on  $p$  and  $z$ . Here  $\vec{\sigma}_1$  and  $\vec{\sigma}_2$  are the spin-vectors of the two nucleons. The subscripts refer to the Central, Spin-spin, Tensor, Spin-Orbit and Quadratic spin-orbit components of the NN T-matrix. Each of these five components occurs in an isoscalar ( $V$ ) and an isovector ( $W$ ) version. Note that, for the purpose of having projection formulas as simple as possible (see eqs.(6-9)), we do not follow the usual conventions for the decomposition of  $\mathcal{T}_{NN}$  in all cases. In particular, we associate the tensor term with the helicity structure  $\vec{\sigma}_1 \cdot \vec{q} \vec{\sigma}_2 \cdot \vec{q}$  in our decomposition. The overall sign of  $\mathcal{T}_{NN}$  is chosen here as it follows directly from the Feynman rules for the S-matrix, with a positive T-matrix, positive phase-shifts and a positive scattering length corresponding to attraction.

We remark that eq.(4) is not just a non-relativistic approximation, but results from the evaluation of the fully relativistic NN T-matrix in the center-of-mass system when reduced to two-component spinors. In principle the NN T-matrix consists of the total sum of all direct diagrams and those with crossed nucleon lines. In practice, there is however no need to evaluate the diagrams with crossed nucleon lines, since the Pauli exclusion principle gives a simple rule, namely  $L + S + I$  being odd, to select the allowed

NN-partial waves. Therefore we identify here  $\mathcal{T}_{NN}$  in eq.(4) only with the sum of all direct diagrams. In the appendix it is shown how to construct from the sum of direct diagrams the complete anti-symmetrized form by application of Fierz-transformations and the substitution  $z \rightarrow -z$ .

In order to compute phase shifts and mixing angles the matrix elements of  $\mathcal{T}_{NN}$  in the  $LSJ$ -basis are needed. To obtain these one first evaluates matrix elements in the helicity basis and then rotates with Wigner d-functions to the  $LSJ$ -basis. We have followed the detailed description in ref. [14] and find with the relevant linear combination in a state with total isospin  $I = 0, 1$ ,

$$U_K = V_K + (4I - 3)W_K, \quad (K = C, S, T, SO, Q) \quad (5)$$

the following projection formulas:

a) Singlet matrix element with  $S = 0$  and  $L = J$ :

$$\langle J0J|\mathcal{T}_{NN}|J0J\rangle = \frac{1}{2} \int_{-1}^1 dz [U_C - 3U_S - q^2 U_T + p^4(z^2 - 1)U_Q] P_J(z). \quad (6)$$

b) Triplet matrix element with  $S = 1$  and  $L = J$ :

$$\begin{aligned} \langle J1J|\mathcal{T}_{NN}|J1J\rangle &= \frac{1}{2} \int_{-1}^1 dz \left\{ 2p^2 [U_{SO} - U_T + p^2 z U_Q] (P_{J+1}(z) + P_{J-1}(z)) \right. \\ &\quad \left. + [U_C + U_S + 2p^2(1+z)U_T - 4p^2 z U_{SO} - p^4(3z^2 + 1)U_Q] P_J(z) \right\}. \end{aligned} \quad (7)$$

c) Triplet matrix elements with  $S = 1$  and  $L = J \pm 1$ :

$$\begin{aligned} \langle J \pm 1, 1J|\mathcal{T}_{NN}|J \pm 1, 1J\rangle &= \frac{1}{2} \int_{-1}^1 dz \left\{ 2p^2 \left[ U_{SO} \pm \frac{1}{2J+1} (U_T - p^2 z U_Q) \right] P_J(z) \right. \\ &\quad \left. + \left[ U_C + U_S + p^2 (p^2(1-z^2)U_Q - 2zU_{SO} \pm \frac{2}{2J+1} (p^2 U_Q - U_T)) \right] P_{J \pm 1}(z) \right\}. \end{aligned} \quad (8)$$

d) Triplet mixing matrix element with  $S = 1$ ,  $L' = J - 1$  and  $L = J + 1$ :

$$\begin{aligned} \langle J - 1, 1J|\mathcal{T}_{NN}|J + 1, 1J\rangle &= \frac{\sqrt{J+1}p^2}{\sqrt{J}(2J+1)} \int_{-1}^1 dz \left\{ (U_T - p^2 U_Q) P_{J+1}(z) \right. \\ &\quad \left. + [(2J - z(2J+1))U_T + p^2 z U_Q] P_J(z) \right\}. \end{aligned} \quad (9)$$

Here,  $P_J(z)$  are ordinary Legendre polynomials of degree  $J$ . In accordance with ref. [14] we did not use the more conventional tensor operator  $3\vec{\sigma}_1 \cdot \hat{q} \vec{\sigma}_2 \cdot \hat{q} - \vec{\sigma}_1 \cdot \vec{\sigma}_2$  in the decomposition of  $\mathcal{T}_{NN}$ , eq.(4), since it leads to unnecessarily complicated projection formulas.

The phase shifts and mixing angles (in the standard convention of Stapp et al. [15]) are then given perturbatively [16] as

$$\delta_{LSJ} = \frac{M^2 p}{4\pi E} \text{Re} \langle LSJ|\mathcal{T}_{NN}|LSJ\rangle, \quad \epsilon_J = \frac{M^2 p}{4\pi E} \text{Re} \langle J - 1, 1J|\mathcal{T}_{NN}|J + 1, 1J\rangle, \quad (10)$$

with the CM nucleon energy  $E = \sqrt{M^2 + p^2}$ . The kinematical prefactor comes from the proper relativistic flux and two-body phase space factors. Since we use chiral perturbation theory here, there is no exact but only a perturbative unitarity. Therefore the calculation of the phase shift according to eq.(10) is valid only as long as the difference between  $\delta$  and  $\sin \delta \cos \delta$  is small. This holds reasonably well for  $|\delta| < 30^\circ$ ; thus with respect to this constraint all NN phase shifts and mixing angles, with the exception of the two S-wave phase shifts, can be calculated reliably in (chiral) perturbation theory.

## IV. ONE LOOP CALCULATION OF THE NN T-MATRIX

In this section we present the analytical results for the NN T-matrix in one-loop approximation. We evaluate the contributions at second and third order of the expansion in powers of small external momenta (here  $p$ ,  $q$  and  $m_\pi$ ). These contributions are divided into three classes: vertex and propagator corrections to one-pion exchange, irreducible two-pion exchange and iterated one-pion exchange. The latter gives rise to a non-vanishing imaginary part in the amplitudes and thus restores unitarity (perturbatively). The possible local NN-contact terms [8] are not considered here, since to the order we are working the corresponding polynomial amplitudes do not contribute to the phase-shifts with  $L \geq 2$  and mixing angles with  $J \geq 2$ .

### A. ONE-PION EXCHANGE

Fig.1 shows the one-pion exchange diagram together with (some) one-loop vertex and propagator corrections to it. We have evaluated all possible diagrams of this sort and found that such one-loop corrections only contribute to mass and coupling constant renormalization. No pion-nucleon "form factor" is generated by any of these diagrams, neither at second nor at third order in the small momentum expansion. Consequently, the one-pion exchange diagrams of Fig.1 lead just to the following well-known contribution to the NN T-matrix,

$$W_T = \frac{g_{\pi N}^2}{4M^2(m_\pi^2 + q^2)}, \quad (11)$$

with  $g_{\pi N}$ ,  $M$ ,  $m_\pi$  the physical values of the pion-nucleon coupling constant, nucleon mass and pion mass. We also note that in the CM frame there are no  $1/M$ -corrections at any order to eq.(11). It is an exact result of the fully relativistic pseudovector (or pseudoscalar)  $\pi NN$ -vertex evaluated in the CM frame. Finally, we remark that the pionic counter terms of  $\mathcal{L}_{\pi\pi}^{(4)}$  in ref. [18] and the on-shell (single) nucleon counter terms of  $\mathcal{L}_{\pi N}^{(3)}$  in ref. [19] do not modify the point-like one-pion exchange eq.(11).

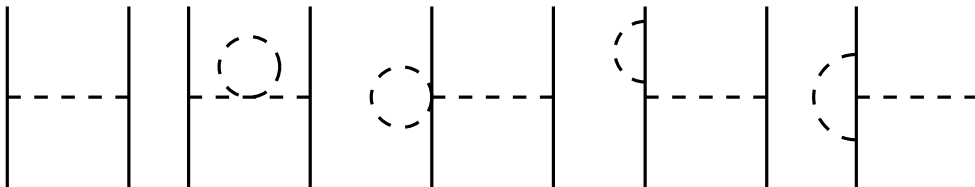


*Fig.1: One-pion exchange, tree-level diagram and diagrams with one-loop corrections*

### B. IRREDUCIBLE TWO-PION EXCHANGE

The two-pion exchange diagrams are shown in Fig.2. Their contributions to the NN T-matrix at second order in small momenta come from insertions of vertices and propagators of the leading order  $\pi N$ -Lagrangian  $\mathcal{L}_{\pi N}^{(1)}$  alone. All these diagrams can be evaluated in a straightforward manner using the heavy baryon formalism of ref. [12], with the exception of the last one, the planar box graph. Here the problem of the so-called pinch singularity

arises [7]. In the heavy mass limit the two nucleon propagators lead to an expression,  $[(l_0 + i\eta)(l_0 - i\eta)]^{-1}$  with infinitesimal  $\eta > 0$ . The integration contour along the real  $l_0$ -axis is pinched between two nearby poles at  $\pm i\eta$ . A loop integral involving this product of propagators does not exist since the two poles at infinitesimal distance  $2\eta$  let the result diverge as  $1/\eta$ . In ref. [7] it was therefore suggested that one should give up covariant perturbation theory and switch over to "old fashioned" time-ordered perturbation theory in order to avoid nearly vanishing energy denominators. This strategy was then carried out in the work of Ordonez, Ray and van Kolck [8].

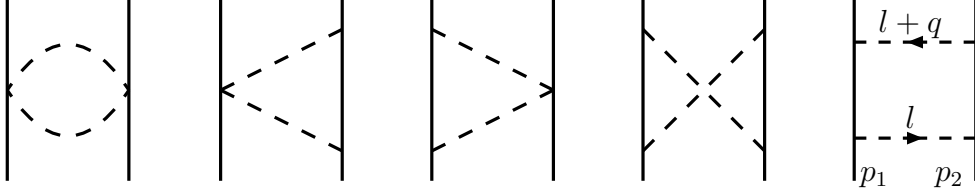


Fig.2: Two-pion exchange diagrams at one-loop order

The abovementioned problem is of purely kinematical origin. It comes from taking the infinite nucleon mass limit  $M \rightarrow \infty$  from the very beginning. In a relativistic calculation with finite nucleon mass  $M$  the planar box diagram is well defined, modulo ultra-violet divergences which can be handled by dimensional regularization. The planar box diagram includes the iterated one-pion exchange which is usually generated by the non-relativistic Lippmann-Schwinger equation in the form  $U^{(1\pi)}\mathcal{G}_{NN}U^{(1\pi)}$  [1]. The non-relativistic two-nucleon propagator  $\mathcal{G}_{NN}$  is the inverse kinetic energy difference (between initial and intermediate state) and thus proportional to the nucleon mass  $M$ . It is exactly this factor of  $M$  in the iterated one-pion exchange which makes the heavy baryon limit of the planar box graph divergent and ill-defined.

The task is to separate off the iterated one-pion exchange proportional to  $M$  and to find the proper irreducible part which then exists in the infinite nucleon mass limit,  $M \rightarrow \infty$ . For that purpose one considers the product of the four relativistic propagators entering the planar box diagram and performs the  $l_0$ -integration via contour methods before doing the  $1/M$ -expansion,

$$\begin{aligned} & \int \frac{dl_0}{2\pi} \frac{4M^2 i}{[(p_1 - l)^2 - M^2 + i\eta][(p_2 + l)^2 - M^2 + i\eta][(l + q)^2 - m_\pi^2 + i\eta][l^2 - m_\pi^2 + i\eta]} \\ &= \frac{M}{[p^2 - (\vec{p} - \vec{l})^2 + i\eta] \omega_1^2 \omega_2^2} + \frac{\omega_1^2 + \omega_1 \omega_2 + \omega_2^2}{2\omega_1^3 \omega_2^3 (\omega_1 + \omega_2)} + \mathcal{O}(M^{-1}). \end{aligned} \quad (12)$$

Here  $p_1^\mu = (E, \vec{p})$ ,  $p_2^\mu = (E, -\vec{p})$  and  $q^\mu = (0, \vec{q})$  are the initial four-momenta of the nucleons (see Fig.2) and the four-momentum transfer in the CM frame,  $\omega_1 = \sqrt{\vec{l}^2 + m_\pi^2}$  and  $\omega_2 = \sqrt{(\vec{l} + \vec{q})^2 + m_\pi^2}$  are the on-shell energies of the two exchanged pions. The factor  $4M^2$  was put into the numerator in order to have the correct heavy baryon limit. In the  $l_0$ -plane the integrand in eq.(12) has eight simple poles, four below and four above the real axis. Two of these poles (one above and one below the real axis) move towards each other for increasing nucleon mass  $M$ . The integral in eq.(12) can be easily evaluated by closing the  $l_0$ -contour e.g. in the lower half-plane and using residue calculus. The first term in the second line of eq.(12), the "iterated one-pion exchange", comes just from that pole which



is moving towards another one. The second term, the "irreducible two-pion exchange", arises from the two poles of the pion propagators. The fourth pole leads to a strongly suppressed contribution of order  $M^{-5}$ . The separation into "iterated one-pion exchange" and "irreducible two-pion exchange" as obtained in eq.(12) is not the standard one of time-ordered perturbation theory, which gives  $-[2\omega_1^2\omega_2^2(\omega_1 + \omega_2)]^{-1}$  for the irreducible part. Nevertheless, eq.(12) is the correct result and it perfectly agrees with the one of time-ordered perturbation theory when performing the systematic  $1/M$ -expansion. Let  $\delta T = [(\vec{p} - \vec{l})^2 - p^2]/2M$  denote the (single) nucleon kinetic energy difference between intermediate and initial (or final) state. From the two irreducible and four reducible time-orderings of the planar box diagram one obtains the following expression for the energy denominators,

$$\begin{aligned} & \frac{1}{4\omega_1\omega_2} \left[ -\frac{2}{(\omega_1 + \omega_2)(\omega_1 + \delta T)(\omega_2 + \delta T)} - \frac{4}{2\delta T(\omega_1 + \delta T)(\omega_2 + \delta T)} \right] \\ &= -\frac{1}{2\delta T \omega_1^2 \omega_2^2} + \frac{\omega_1^2 + \omega_1 \omega_2 + \omega_2^2}{2\omega_1^3 \omega_2^3 (\omega_1 + \omega_2)} + \mathcal{O}(\delta T), \end{aligned} \quad (13)$$

including the phase space density factor  $(4\omega_1\omega_2)^{-1}$ .

One can apply the previous method to the crossed box diagram as well and finds as a result (in the  $M \rightarrow \infty$  limit) the same irreducible part as in eq.(12) but with opposite sign. In the previous analysis the momentum dependence of the  $\pi NN$ -coupling was not included. However, in a leading non-relativistic approximation it is of the form  $\vec{\sigma} \cdot \vec{l}$  and does therefore not interfere with the  $l_0$ -integration.

As a result one finds that the isoscalar central amplitude  $V_C$  adds up to zero for the sum of planar and crossed box graphs. For the isovector central amplitude  $W_C$  there is a further relative minus sign from the isospin factors, which are  $3 - 2\vec{\tau}_1 \cdot \vec{\tau}_2$  for the planar box and  $3 + 2\vec{\tau}_1 \cdot \vec{\tau}_2$  for the crossed box. To the amplitude  $W_C$  the two diagrams contribute with equal sign. In the spin-spin and tensor channels the situation concerning relative signs is just reverse, due to a further relative sign between planar and crossed box graph coming from the different ordering of  $\vec{\sigma}$ -matrices. Altogether, one finds from the graphs in Fig.2 the following (renormalized) contributions to the NN T-matrix from irreducible two-pion exchange at second order in small momenta,

$$\begin{aligned} W_C = & \frac{1}{384\pi^2 f_\pi^4} \left\{ \left[ 6m_\pi^2(15g_A^4 - 6g_A^2 - 1) + q^2(23g_A^4 - 10g_A^2 - 1) \right] \ln \frac{m_\pi}{\lambda} \right. \\ & + 4m_\pi^2(4g_A^4 + g_A^2 + 1) + \frac{q^2}{6}(5g_A^4 + 26g_A^2 + 5) \\ & \left. + \left[ 4m_\pi^2(5g_A^4 - 4g_A^2 - 1) + q^2(23g_A^4 - 10g_A^2 - 1) + \frac{48g_A^4 m_\pi^4}{4m_\pi^2 + q^2} \right] L(q) \right\}, \end{aligned} \quad (14)$$

$$V_T = -\frac{1}{q^2} V_S = \frac{3g_A^4}{64\pi^2 f_\pi^4} \left\{ \ln \frac{m_\pi}{\lambda} - \frac{1}{2} + L(q) \right\}, \quad (15)$$

with the logarithmic loop function

$$L(q) = \frac{w}{q} \ln \frac{w+q}{2m_\pi}, \quad w = \sqrt{4m_\pi^2 + q^2}. \quad (16)$$

The NN-amplitudes not specified in eqs.(14,15) are zero. The first two lines in eq.(14) for  $W_C$  and the constant terms in eq.(15) for  $V_T$  do not contribute to phase shifts with  $L \geq 2$

and mixing angles with  $J \geq 2$ . Such polynomials in  $q^2$  drop out of the projection formulas eqs.(6-9) by orthogonality of the  $P_J(z)$ . Therefore the value of the (a priori arbitrary) renormalization scale  $\lambda$  is irrelevant in this work.

Next we consider the two-pion exchange contributions at third order in the small momentum expansion. These arise from the one-loop diagrams in Fig.2 with exactly one insertion from the next-to-leading order  $\pi N$ -Lagrangian  $\mathcal{L}_{\pi N}^{(2)}$ . The contributions are either proportional to the low-energy constants  $c_i$  or they carry a suppression factor  $1/M$ . Again, all but the planar box graph can be evaluated in straightforward manner using the heavy baryon formalism [12]. The planar box graph requires a special treatment in order to obtain correctly all  $1/M$ -corrections. First, the expansion of the propagator integral, eq.(12), in powers of  $1/M$  has to be performed one order further. This gives rise to new irreducible pieces (proportional to  $1/M$ ) and a relativistic correction factor,  $1 - p^2/2M^2 \simeq M/E$ , to the iterated one-pion exchange. Secondly, one has to expand in powers of  $1/M$  the product of pseudovector  $\pi NN$ -vertices and  $(\not{p} + M)/2M$ -factors from the nucleon propagators sandwiched between in- and out-going Dirac spinors. At order  $1/M$ , only terms proportional to  $l_0$  and  $l_0^3$  are generated this way. The integral analogous to eq.(12) with an additional factor  $l_0$  or  $l_0^3$  in the numerator gives zero,  $0 + \mathcal{O}(M^{-2})$ . At order  $1/M^2$  terms independent of  $l_0$  but proportional to  $\vec{l} \cdot (2\vec{p} - \vec{l})$  appear. Together with eq.(12) these give rise to a further  $1/M$ -correction to the irreducible two-pion-exchange. With these techniques and the rules of dimensional regularization to evaluate the remaining  $d^3l$ -integral one obtains all  $1/M$ -corrections coming from the planar box graph. As a check we applied the same technique to the crossed box and triangle graphs. In all cases we found perfect agreement with the results obtained independently using the heavy baryon formalism. This shows that our method of doing first the  $l_0$ -integral and then expanding in  $1/M$ , which is necessary for a systematic evaluation of the planar box diagram, is indeed correct. Putting all pieces together, we finally arrive after tedious calculation at the following irreducible two-pion exchange contributions to the NN T-matrix at third order in small momenta,

$$V_C = \frac{3g_A^2}{16\pi f_\pi^4} \left\{ 4(c_1 - c_3)m_\pi^3 - \frac{g_A^2 m_\pi}{16M}(m_\pi^2 + 3q^2) - \frac{g_A^2 m_\pi^5}{16M(4m_\pi^2 + q^2)} \right. \\ \left. - c_3 m_\pi q^2 + \left[ 2m_\pi^2(2c_1 - c_3) - q^2 \left( c_3 + \frac{3g_A^2}{16M} \right) \right] (2m_\pi^2 + q^2) A(q) \right\}, \quad (17)$$

with a new loop function

$$A(q) = \frac{1}{2q} \arctan \frac{q}{2m_\pi}, \quad (18)$$

$$W_C = \frac{g_A^2}{128\pi M f_\pi^4} \left\{ (8 - 11g_A^2)m_\pi^3 + (2 - 3g_A^2)m_\pi q^2 - \frac{3g_A^2 m_\pi^5}{4m_\pi^2 + q^2} \right. \\ \left. + [4m_\pi^2 + 2q^2 - g_A^2(4m_\pi^2 + 3q^2)](2m_\pi^2 + q^2) A(q) \right\}, \quad (19)$$

$$V_T = -\frac{1}{q^2} V_S = -\frac{9g_A^4}{512\pi M f_\pi^4} \left\{ m_\pi + (2m_\pi^2 + q^2) A(q) \right\}, \quad (20)$$

$$W_T = -\frac{1}{q^2} W_S = \frac{g_A^2}{32\pi f_\pi^4} \left\{ \left( c_4 + \frac{2 - 3g_A^2}{8M} \right) m_\pi \right.$$

$$+ \left[ \left( c_4 + \frac{1}{4M} \right) (4m_\pi^2 + q^2) - \frac{g_A^2}{8M} (10m_\pi^2 + 3q^2) \right] A(q) \Big\}, \quad (21)$$

$$V_{SO} = \frac{3g_A^4}{64\pi M f_\pi^4} \left\{ m_\pi + (2m_\pi^2 + q^2) A(q) \right\}, \quad (22)$$

$$W_{SO} = \frac{g_A^2(1 - g_A^2)}{64\pi M f_\pi^4} \left\{ m_\pi + (4m_\pi^2 + q^2) A(q) \right\}. \quad (23)$$

Note that the  $c_1$ -part of  $V_C$  in eq.(17) is proportional to the one-loop contribution to the nucleon scalar form factor, namely  $-8c_1 f_\pi^{-2} \sigma_N(-q^2)_{loop}$  [20] and the low-energy constant  $c_3$  is related to the so-called nucleon axial polarizability [12,17],  $\alpha_A = -2c_3/f_\pi^2 - g_A^2 m_\pi (48g_A^2 + 77)/(384\pi f_\pi^4) = 6.44 \text{ fm}^3$  which is governed by virtual  $\Delta$ -isobar excitation. Similarly, the  $c_4$ -part of  $W_T$  in eq.(21) is proportional to the one-loop contribution to the nucleon isovector magnetic form factor (normalized to  $1 + \kappa_p - \kappa_n$ ), namely  $-(c_4/4M f_\pi^2) G_M^V(-q^2)_{loop}$ . The low-energy constant  $c_2$  is absent in the above expressions. In the actual calculation one sees that this comes from the fact that the energy transfer in the CM frame is zero,  $q_0 = 0$ . We note that all contributions at third order in small momenta are finite (free of divergences). This is consistent with the fact that no local counter terms (analytic in the quark mass) exist at this order of the small momentum expansion to cancel divergences. The spin-orbit amplitudes  $V_{SO}$ ,  $W_{SO}$  generated by chiral two-pion exchange are proportional to  $1/M$ . This is different from the OBE-model, where scalar and vector meson exchange lead to spin-orbit terms proportional to  $1/M^2$ . Furthermore, to the order we are working, there is no quadratic spin-orbit contribution from irreducible graphs. Such terms are suppressed by a factor  $1/M^2$ . Already a short glance at the analytical formulas, eqs.(14-23) for the two-pion exchange contributions shows that these are all increasing (in magnitude) with increasing momentum transfer  $q$ . This is in contrast to the OBE-model, where by construction all NN-potentials decrease as a function of  $q$ . The growth in  $q$  of the chiral two-pion exchange potentials is a consequence of the Goldstone boson nature of the pion. A Goldstone boson has (and induces) weak interaction at low energies and stronger interaction at higher energies (see also the explicit expressions for the one-loop  $\pi N$ -scattering amplitude in ref. [10] and the one-loop  $\pi\pi$ -scattering amplitude in ref. [18], which share the same property). However, in many model calculations, this feature is altered by the introduction of phenomenological cut-offs, form factors and the like.

### C. ITERATED ONE-PION EXCHANGE

The planar box graph includes the iterated one-pion exchange, which is enhanced by a factor  $M$ . Even though we counted the diagram naively as second order in small momenta, the actual contribution to the NN T-matrix is of first order in small momenta. The occurrence of such a large scale enhancement factor  $M$  in iterated diagrams changes the correspondence between the loop expansion and the small momentum expansion for processes involving two (or more) nucleons. Ladder diagrams with  $n$  loops contribute already at  $n$ -th order in the small momentum expansion, whereas the naive counting rules would classify them as order  $2n$ . The iterated one-pion exchange including the relativistic correction factor  $M/E$  has the following integral representation,

$$\frac{g_A^4 M^2}{16 E f_\pi^4} (2 \vec{\tau}_1 \cdot \vec{\tau}_2 - 3) \int \frac{d^3 l}{(2\pi)^3} \frac{\vec{\sigma}_1 \cdot (\vec{l} + \vec{p}') \vec{\sigma}_2 \cdot (\vec{l} + \vec{p}') \vec{\sigma}_1 \cdot (\vec{l} + \vec{p}) \vec{\sigma}_2 \cdot (\vec{l} + \vec{p})}{(p^2 - l^2 + i\eta)[(\vec{l} + \vec{p}')^2 + m_\pi^2][(\vec{l} + \vec{p})^2 + m_\pi^2]}. \quad (24)$$

The isospin factor  $8I - 9$  suppresses the contribution to  $(I = 1)$ -states by a factor  $1/9$  compared to  $(I = 0)$ -states. The resulting three-dimensional integrals can be evaluated in closed form, and the contributions to the NN T-matrix are expressed in terms of the following set of complex-valued functions,

$$\Gamma_0(p) = \frac{1}{2p} \left[ \arctan \frac{2p}{m_\pi} + i \ln \frac{u}{m_\pi} \right], \quad u = \sqrt{m_\pi^2 + 4p^2}, \quad (25)$$

$$\Gamma_1(p) = \frac{1}{2p^2} \left[ m_\pi + ip - (m_\pi^2 + 2p^2) \Gamma_0(p) \right], \quad (26)$$

$$G_0(p, q) = \frac{1}{qR} \left[ \arcsin \frac{qm_\pi}{uw} + i \ln \frac{pq + R}{um_\pi} \right], \quad R = \sqrt{m_\pi^4 + p^2 w^2}, \quad (27)$$

$$G_1(p, q) = \frac{\Gamma_0(p) - 2A(q) - (m_\pi^2 + 2p^2)G_0(p, q)}{4p^2 - q^2}, \quad (28)$$

$$G_2(p, q) = p^2 G_0(p, q) + (m_\pi^2 + 2p^2)G_1(p, q) + A(q), \quad (29)$$

$$G_3(p, q) = \frac{\frac{1}{2}\Gamma_1(p) - p^2 G_0(p, q) - 2(m_\pi^2 + 2p^2)G_1(p, q)}{4p^2 - q^2}, \quad (30)$$

with  $w$  and  $A(q)$  given in eqs.(16,18). Note that the functions  $G_{1,2,3}(p, q)$  are not singular at  $z = -1$  or  $q^2 = 4p^2$ . In terms of these complex functions the contributions to the NN T-matrix read,

$$W_C = -\frac{2}{3}V_C = \frac{g_A^4 M^2}{128\pi E f_\pi^4} \left\{ 4(2m_\pi^2 + q^2)\Gamma_0(p) + 2q^2\Gamma_1(p) - 4ip - (2m_\pi^2 + q^2)^2 G_0(p, q) \right\}, \quad (31)$$

$$W_T = -\frac{2}{3}V_T = -\frac{1}{q^2}W_S = \frac{2}{3q^2}V_S = -\frac{g_A^4 M^2}{32\pi E f_\pi^4} G_2(p, q), \quad (32)$$

$$W_{SO} = -\frac{2}{3}V_{SO} = \frac{g_A^4 M^2}{64\pi E f_\pi^4} \left\{ -2\Gamma_0(p) - 2\Gamma_1(p) + (2m_\pi^2 + q^2)[G_0(p, q) + 2G_1(p, q)] \right\}, \quad (33)$$

$$W_Q = -\frac{2}{3}V_Q = \frac{g_A^4 M^2}{32\pi E f_\pi^4} \left\{ G_0(p, q) + 4G_1(p, q) + 4G_3(p, q) \right\}. \quad (34)$$

Here, for the first time a non-vanishing quadratic spin-orbit contribution is found. Using dimensional regularization, we find that the iterated one-pion exchange is finite and has no divergences. Note that the contributions of iterated one-pion exchange, eqs.(31-34), depend on both kinematical variables  $p$  and  $q$ , whereas irreducible two-pion exchange, eqs.(14-23), depends only on the momentum transfer  $q$ . To the order we are working the iterated one-pion exchange is the only contribution to the NN T-matrix with a non-vanishing imaginary part and thus it restores unitarity to this order. In partial waves this imaginary part is given by the square of the phase-shift calculated from one-pion exchange, eq.(11); in the case of the mixing triplet states with  $L = J \pm 1$  it is actually a quadratic expression in these phase shifts and the mixing angle. Therefore the imaginary part of iterated one-pion exchange allows for a numerical check of unitarity, which actually serves as a check of both, the analytical expressions for iterated one-pion exchange, eqs.(31-34) and the projection formulas, eqs.(6-9). We have found that in all cases this numerical

check of unitarity works at an accuracy  $10^{-4}$  or better. Furthermore, we have verified analytically that the optical theorem is satisfied. It equates the imaginary part of the NN T-matrix in forward direction (only  $V_C$  and  $W_C$  in eq.(31) contribute) to  $pE/M^2$  times the (unpolarized) total NN-cross section calculated in (non-relativistic) one-pion exchange approximation without crossed nucleon lines.

Since each iteration of one-pion exchange brings a further enhancement factor  $M$ , up to three iterations will contribute to the NN T-matrix calculated completely to third order in small momenta. This corresponds to two- and three-loop diagrams which are extremely difficult to evaluate. Numerically, we find that in most cases iterated one-pion exchange is small compared to irreducible two-pion exchange. We can therefore assume that the higher order iterations can be neglected.

At zeroth order in the small momentum expansion, not only one-pion exchange eq.(11) contributes to the NN T-matrix, but also contact terms of the (Fierz-antisymmetric) form,

$$3B + B' \vec{\tau}_1 \cdot \vec{\tau}_2 - (2B + B') \vec{\sigma}_1 \cdot \vec{\sigma}_2 - B \vec{\tau}_1 \cdot \vec{\tau}_2 \vec{\sigma}_1 \cdot \vec{\sigma}_2. \quad (35)$$

In tree approximation eq.(35) gives a contribution to the two S-wave amplitudes only. At one-loop order the iteration of this contact interaction and diagrams with an additional pion exchange occur. We have checked that the one-loop diagrams involving the lowest order contact interaction eq.(35) do not contribute to the phase-shifts with  $L \geq 2$  and the mixing angles with  $J \geq 2$ . Therefore, we do not need to specify the constants  $B, B'$  in eq.(35).

This completes the discussion of the NN T-matrix in one-loop approximation. We find that if we restrict ourselves to the phase-shifts with  $L \geq 2$  and mixing angles with  $J \geq 2$  (peripheral partial waves), not even a single adjustable parameter shows up. To the order we are working this peripheral part of the NN T-matrix involves only well-known physical parameters such as  $g_{\pi N}$ ,  $f_\pi$ ,  $m_\pi$ ,  $M$  and three low-energy constants  $c_{1,3,4}$  which are well determined from  $\pi N$ -scattering data. Such features allow for a clean test of chiral symmetry in NN-interaction.

## V. RESULTS AND DISCUSSION

In this section we present and discuss our results for the phase-shifts with  $L \geq 2$  and mixing angles with  $J \geq 2$  up to nucleon laboratory kinetic energies of  $T_{lab} = 280$  MeV, the  $NN\pi^0$ -threshold. At such an energy, momentum transfers up to  $q = 5.25 m_\pi = 725$  MeV are involved, which are quite large for the application of chiral perturbation theory. Despite this fact, we present here results up to the  $NN\pi^0$ -threshold, in order to demonstrate where our model independent predictions are in agreement with existing data and where deviations show up. For the sake of completeness, we summarize again the values of the physical parameters used in the calculation:  $f_\pi = 92.4$  MeV,  $g_{\pi N} = 13.4$  as determined from  $\pi N$ -dispersion analysis [13],  $m_\pi = 138$  MeV,  $M = 939$  MeV for the average pion and nucleon mass and the central values of the low-energy constants,  $c_1 = -0.9$  GeV $^{-1}$ ,  $c_3 = -5.3$  GeV $^{-1}$  and  $c_4 = 3.6$  GeV $^{-1}$  [10].

## A. D-WAVES

The D-wave phase shifts and mixing angle  $\epsilon_2$  are shown in Fig.3. The dashed curve corresponds to the one-pion exchange approximation and the full curve includes in addition two-pion exchanges (irreducible two-pion exchange and iterated one-pion exchange). The dotted and dashed-dotted curves represent the empirical NN phase shift analyses of ref. [4] and ref. [21] (as far as available), respectively. In all cases the model independent two-pion exchange corrections go into the proper direction, but they tend to be too large, already at small  $T_{lab}$ . The one-loop predictions for the D-wave phase shifts deviate appreciably from the data. An exception is the mixing angle  $\epsilon_2$  which is well reproduced up to  $T_{lab} = 120$  MeV. The  $2\pi$ -exchange tensor force in this channel has the correct sign. However, it grows too strongly with energy and even overcompensates the  $1\pi$ -exchange tensor force at the  $NN\pi^0$ -threshold. The  ${}^3D_1$  phase shift is also in fair agreement with the data up to  $T_{lab} = 200$  MeV. This results from an almost complete cancelation of irreducible two-pion exchange and iterated one-pion exchange contributions. Above  $T_{lab} = 200$  MeV this cancelation mechanism does not work anymore. The good agreement between the data and the one-pion exchange approximation in the  ${}^3D_1$  partial wave is contrary to expectations and appears accidental, since in G-waves (see later) there are still sizeable differences between data and one-pion exchange approximation. From all this we conclude that one-pion and two-pion exchange alone are not sufficient to describe the dynamics in the NN D-waves [5] (see also the discussion of the coordinate potentials in the next section). Obviously, strong cancelations between  $2\pi$ -exchange and  $3\pi$ -exchange together with shorter range effects are taking place here. The latter ingredients of the NN T-matrix go beyond the one-loop approximation.

## B. F-WAVES

The F-wave phase shifts and the mixing angle  $\epsilon_3$  are shown in Fig.4. Again, the  $2\pi$ -exchange corrections to  $1\pi$ -exchange go into the right direction. The predictions for the phase-shifts in the  ${}^1F_3$  and  ${}^3F_3$  partial waves are in good agreement with existing data up to  $T_{lab} = 180$  MeV. At larger energies the  $2\pi$ -exchange effects become again too strong. In the  ${}^3F_2$  partial wave we find a correction to  $1\pi$ -exchange opposite to the trend of the data of ref. [21]. The latest fit of the  ${}^3F_2$  phase shift from the VPI group [4] (not shown) is very similar to the one of ref. [21]. The mixing angle  $\epsilon_3$ , however, is in perfect agreement with the data of ref. [4,21] for all energies up to the  $NN\pi^0$ -threshold at  $T_{lab} = 280$  MeV. To this observable irreducible  $2\pi$ -exchange and iterated  $1\pi$ -exchange contribute with almost equal strength. Note that the empirical F-wave phase-shifts are quite small, namely less than  $4.5^\circ$ . It would be very interesting to see how the present discrepancies between the chiral NN F-wave phase shifts and the existing analyses reflect themselves in a direct comparison with scattering data, i.e. differential cross sections and polarization observables. Unfortunately, we can not present such a direct comparison here.

### C. G-WAVES

The G-wave phase shifts and the mixing angle  $\epsilon_4$  are shown in Fig.5. The chiral predictions are in good agreement with data for all four partial wave phase shifts and the mixing angle up to  $T_{lab} = 220$  MeV. Note that the differences between  $1\pi$ -exchange and data are still sizeable in the  $^1G_4$  and  $^3G_5$  partial waves. The model independent chiral  $2\pi$ -exchange corrections have indeed the correct sign and magnitude to close this gap between data and  $1\pi$ -exchange approximation. In the  $^1G_4$  partial wave the correction comes mainly from irreducible  $2\pi$ -exchange, whereas in the  $^3G_5$  partial wave (with  $I = 0$ ) both irreducible  $2\pi$ -exchange and iterated  $1\pi$ -exchange contribute with roughly equal strength. For the  $^3G_3$  and  $^3G_4$  phase shifts and  $\epsilon_4$  the  $2\pi$ -exchange corrections are quite small. Nevertheless, these small effects improve the agreement between data and chiral predictions.

### D. H-WAVES

The H-wave phase shifts and the mixing angle  $\epsilon_5$  are shown in Fig.6. The corrections due to  $2\pi$ -exchange are already quite small and they follow the trend of the data. An exception is the  $^3H_4$  phase shift where we find a very small positive contribution. However, the empirical  $^3H_4$  phase shifts are very small, less than  $0.5^\circ$ , and the difference between the existing phase shift analyses and the chiral prediction may be insignificant if one compares directly the NN-scattering data.

### E. I-WAVES

The I-wave phase shifts and the mixing angle  $\epsilon_6$  are shown in Fig.7. Again, the corrections coming from  $2\pi$ -exchange are quite small and they follow the trend of the data. Altogether, we find a faster convergence to the  $1\pi$ -exchange approximation in the high angular momentum partial waves as obtained in the existing NN phase-shift analyses. The calculation in chiral perturbation theory presented here is most reliable in the high angular momentum partial waves. These are the ones which probe the long and medium range parts of the NN-interaction which are built in here in a model independent way via  $1\pi$ - and chiral  $2\pi$ -exchange. In the existing phase shift analysis the (small) effects in high angular momentum partial waves may result mainly from effective potentials [4,21] fitted to lower partial waves with only limited direct constraints from the NN-scattering data.

FIGURES

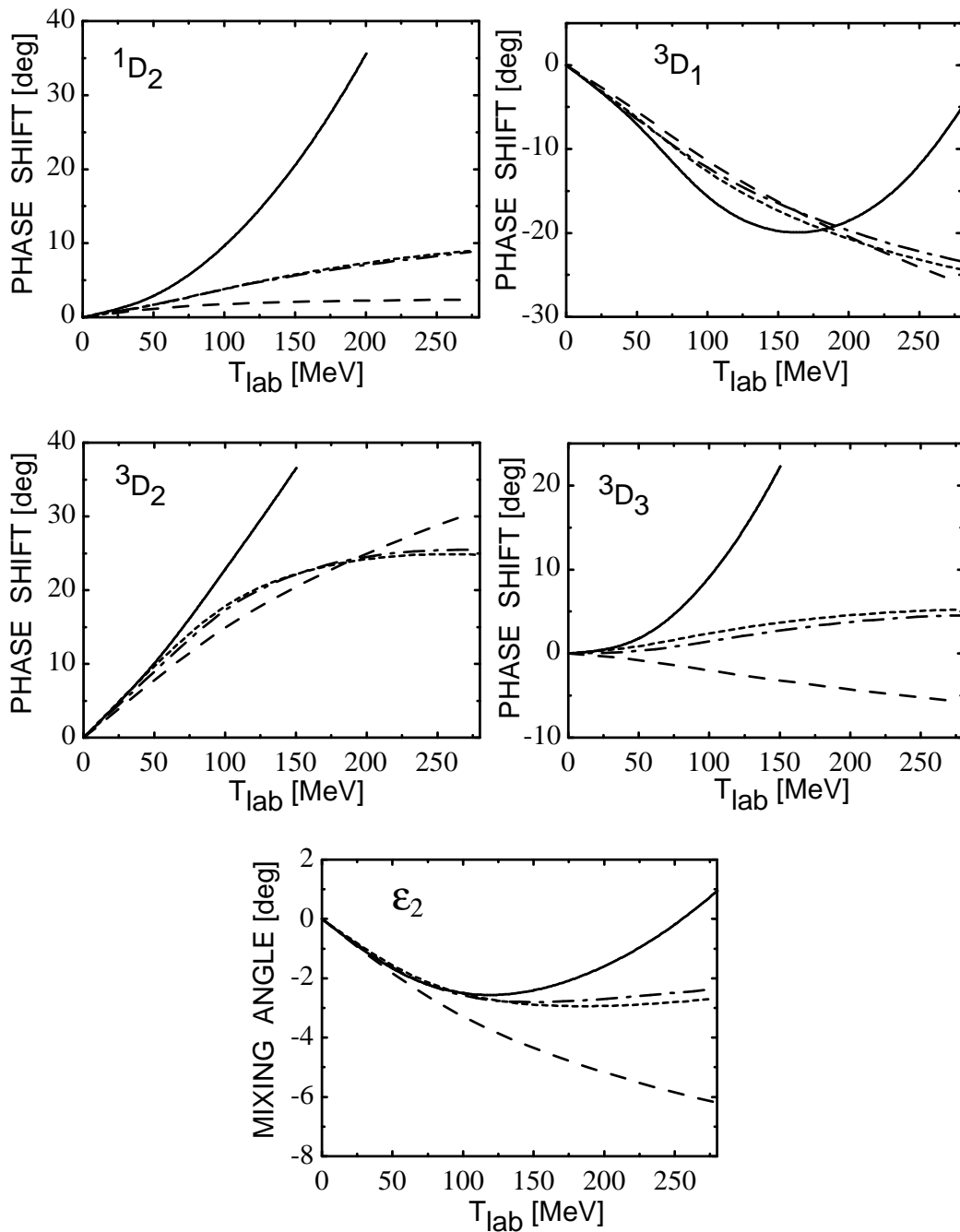


Fig.3: D-wave NN phase shifts and mixing angle  $\epsilon_2$  versus the nucleon laboratory kinetic energy  $T_{\text{lab}}$ . The dashed curve corresponds to the  $1\pi$ -exchange approximation and full curve includes chiral  $2\pi$ -exchange as well. The dotted and dashed-dotted curves represent the empirical NN phase shift analyses of ref. [4] and ref. [21], respectively.



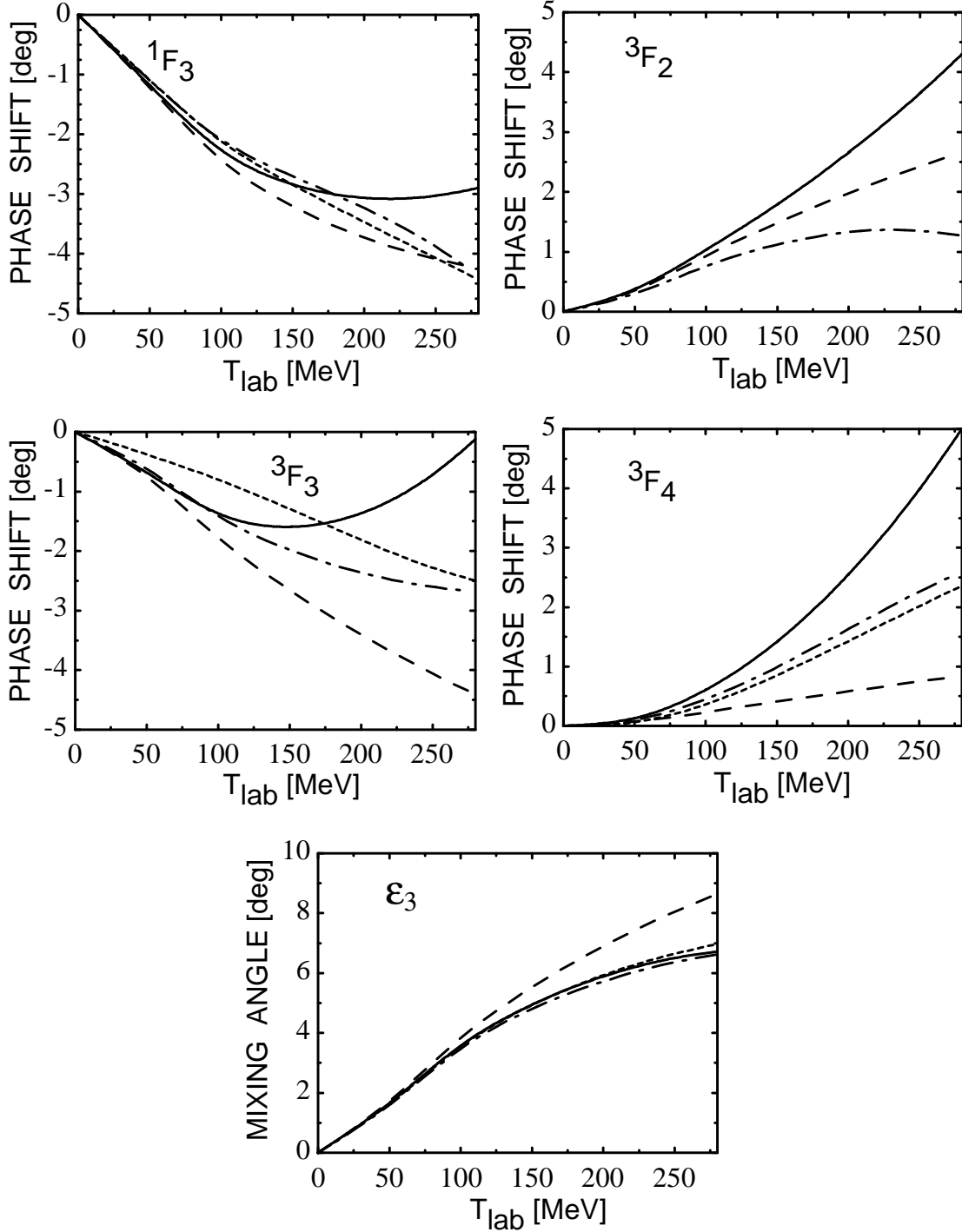


Fig.4:  $F$ -wave  $NN$  phase shifts and mixing angle  $\epsilon_3$  versus the nucleon laboratory kinetic energy  $T_{lab}$ . For notation see Fig.3.

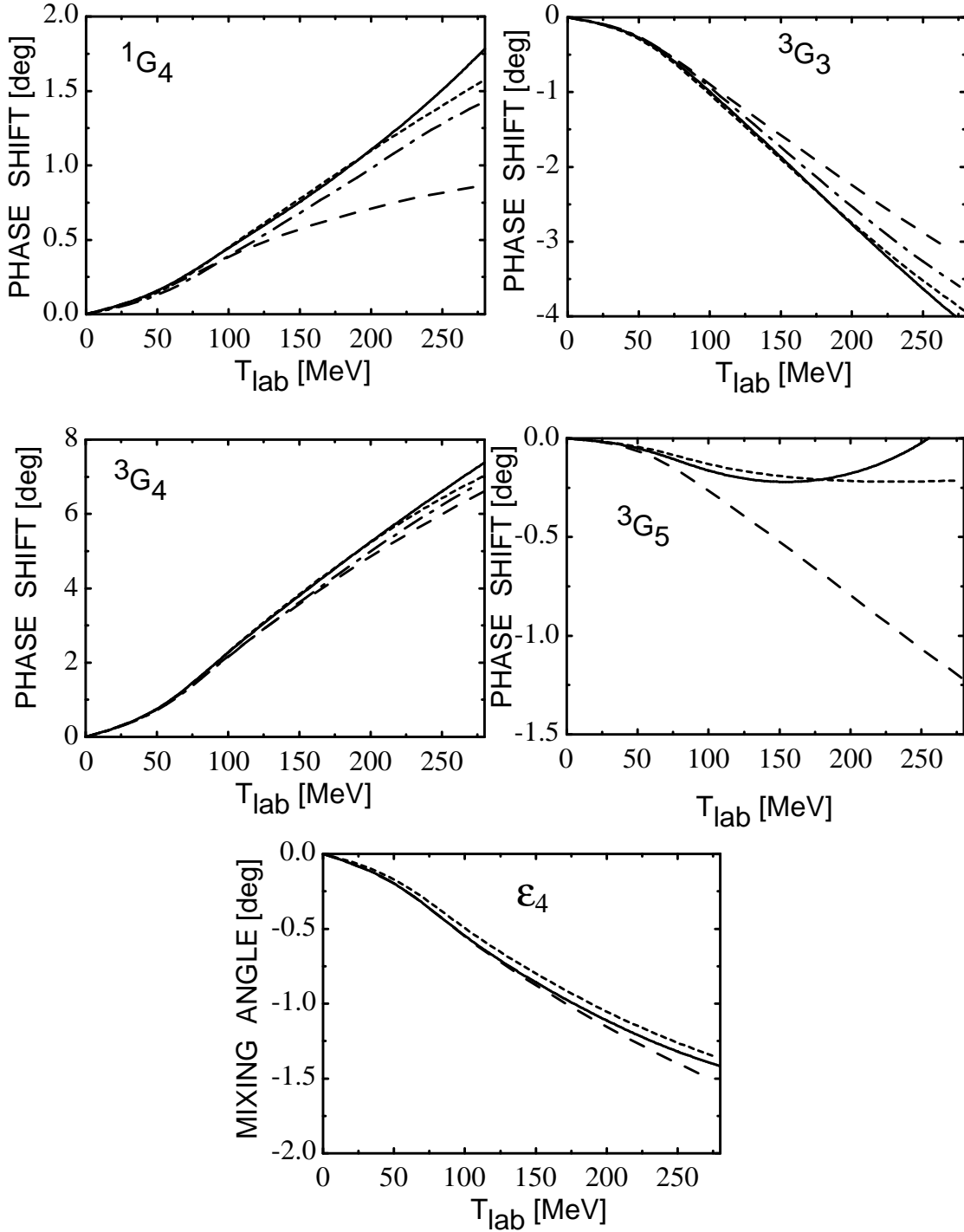


Fig.5:  $G$ -wave NN phase shifts and mixing angle  $\epsilon_4$  versus the nucleon laboratory kinetic energy  $T_{lab}$ . For notation see Fig.3.

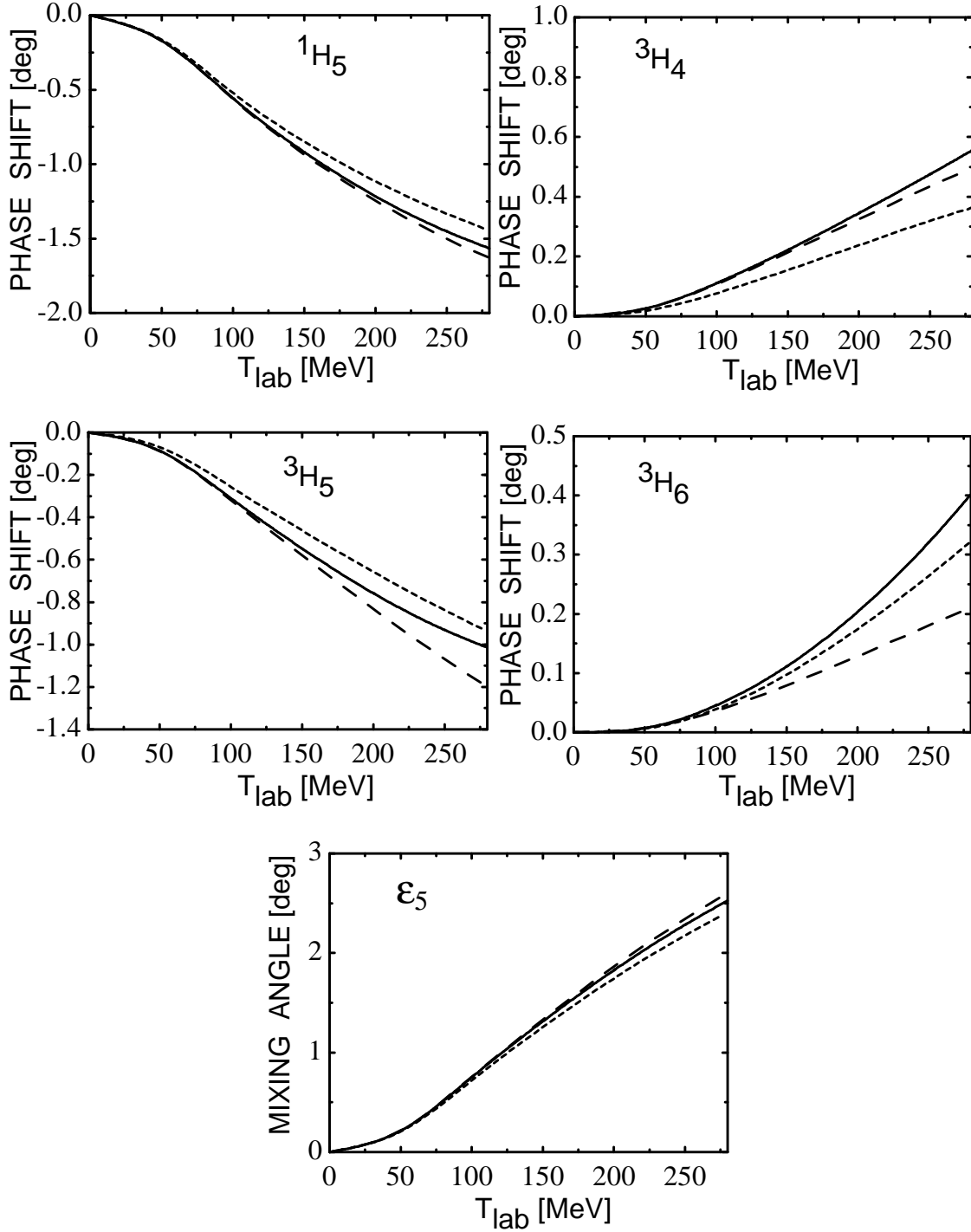


Fig.6:  $H$ -wave  $NN$  phase shifts and mixing angle  $\epsilon_5$  versus the nucleon laboratory kinetic energy  $T_{\text{lab}}$ . For notation see Fig.3.

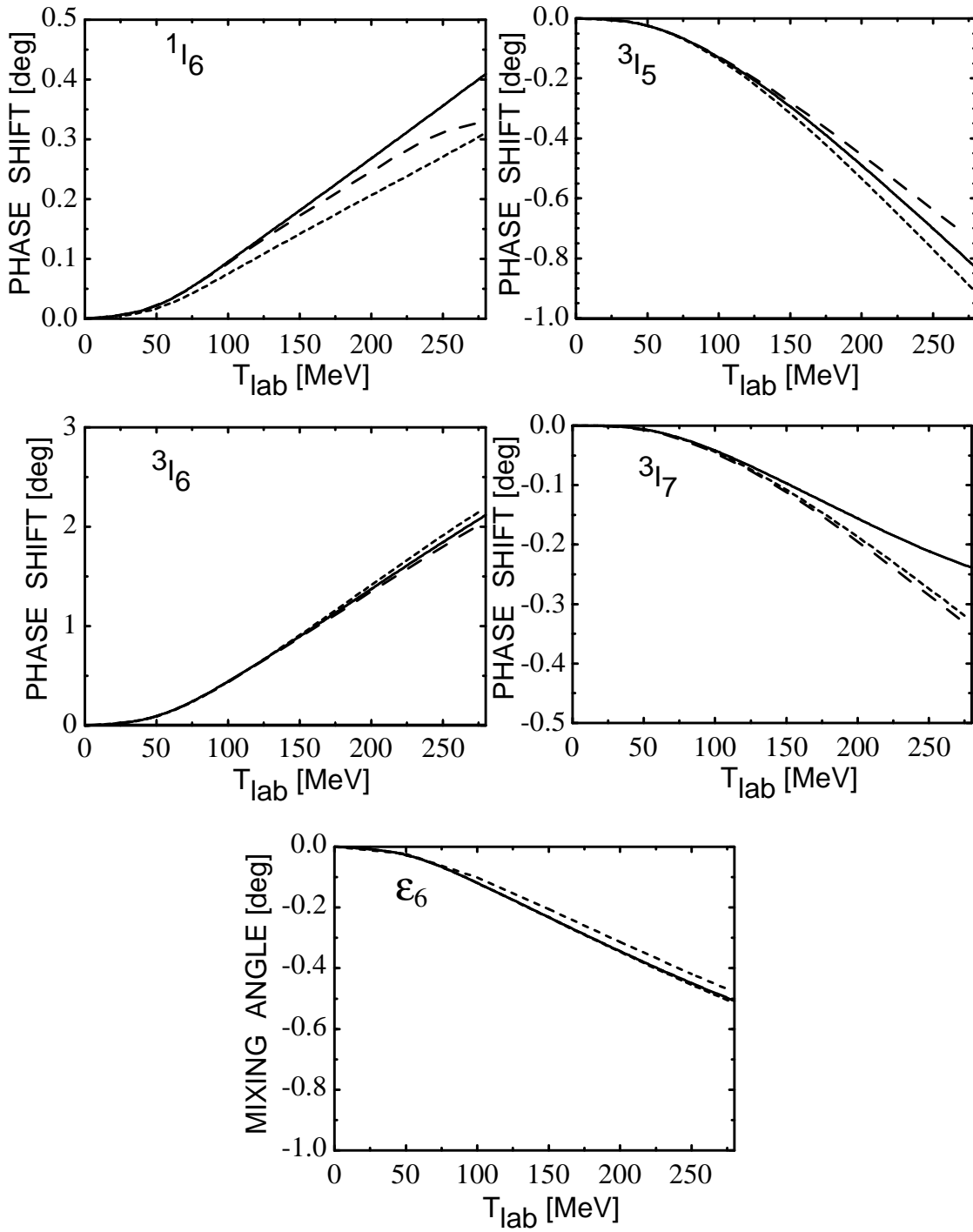


Fig. 7: I-wave NN phase shifts and mixing angle  $\epsilon_6$  versus the nucleon laboratory kinetic energy  $T_{\text{lab}}$ . For notation see Fig.3.

## VI. COORDINATE SPACE REPRESENTATIONS

In order to interpret the effects of irreducible chiral two-pion exchange and to compare with phenomenological approaches it is desirable to have a coordinate space representation of the corresponding potentials. However an ordinary inverse Fourier-transform of the momentum space functions given in section IIB is not possible, because of their growth with  $q$ . In this case the coordinate space representation of the finite range parts can be obtained in the form of a continuous superposition of Yukawa functions [1]. The mass spectrum entering in this representation is given by the imaginary part of the momentum space functions analytically continued to time-like momentum transfer,  $q = 0^+ - i\mu$ . For the isoscalar central potential in  $r$ -space one has then the following spectral representation,

$$\tilde{V}_C(r) = -\frac{1}{2\pi^2 r} \int_{2m_\pi}^{\infty} d\mu \mu e^{-\mu r} \text{Im} V_C(-i\mu) . \quad (36)$$

Using  $\text{Im} A(-i\mu) = (\pi/4\mu)\theta(\mu - 2m_\pi)$  for the relevant loop function (note that due to the coalescence of normal threshold  $\mu_0 = 2m_\pi$  and anomalous threshold  $\mu_c = \sqrt{4m_\pi^2 - m_\pi^4/M^2} = 1.995m_\pi$  in the heavy nucleon limit, this imaginary part starts with a non-zero value at threshold) one finds the following closed expression for the isoscalar central potential,

$$\begin{aligned} \tilde{V}_C(r) = \frac{3g_A^2}{32\pi^2 f_\pi^4} \frac{e^{-2x}}{r^6} \left\{ \left( 2c_1 + \frac{3g_A^2}{16M} \right) x^2 (1+x)^2 + \frac{g_A^2 x^5}{32M} \right. \\ \left. + \left( c_3 + \frac{3g_A^2}{16M} \right) (6 + 12x + 10x^2 + 4x^3 + x^4) \right\} \end{aligned} \quad (37)$$

with the abbreviation  $x = m_\pi r$ . Since  $c_{1,3} + 3g_A^2/16M < 0$ , this potential is attractive for all distances  $r$  as expected. Its asymptotic behaviour for large  $r$  is a modified Yukawa function with twice the pion mass,  $e^{-2m_\pi r}/r^2$ , neglecting the small  $1/M$ -terms. At a distance  $r = 1/m_\pi = 1.43$  fm one finds an attraction of  $\tilde{V}_C(1.43\text{fm}) = -35.9$  MeV. This number is twice as large as the attraction produced by the fictitious  $\sigma(550)$ -boson of the Bonn potential [1,5].

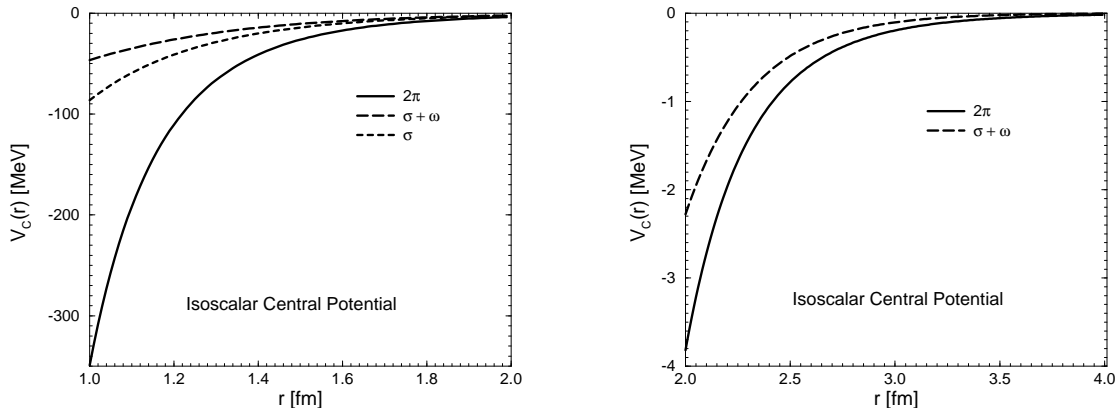


Fig.8: The isoscalar central potential  $\tilde{V}_C(r)$  generated by irreducible chiral two-pion exchange in  $r$ -space (full line). The dashed lines show the phenomenological  $\sigma + \omega$  and  $\sigma$ -contributions.

In Fig.8 we show the isoscalar central potential  $\tilde{V}_C(r)$  for  $1 \text{ fm} < r < 2 \text{ fm}$  and  $2 \text{ fm} < r < 4 \text{ fm}$ . Our results are qualitatively in agreement with the recent work of ref. [23],

but their isoscalar central NN-potential is even somewhat more attractive. The terms proportional to  $c_{1,3}$  in eq.(37) agree with the earlier work of [24] up to the isospin factor 3 which was inadvertently omitted in [24]. Furthermore it is interesting to observe that in the chiral limit  $m_\pi = 0$  the isoscalar central two-pion exchange potential shows a  $1/r^6$  fall-off which is typical for a non-relativistic Van-der-Waals potential.

The spectral representation of the isovector tensor potential (accompanying the standard tensor operator  $3\vec{\sigma}_1 \cdot \hat{r} \vec{\sigma}_2 \cdot \hat{r} - \vec{\sigma}_1 \cdot \vec{\sigma}_2$ ) takes a similar form,

$$\widetilde{W}_T(r) = \frac{1}{6\pi^2 r^3} \int_{2m_\pi}^{\infty} d\mu \mu e^{-\mu r} (3 + 3\mu r + \mu^2 r^2) \text{Im} W_T(-i\mu) . \quad (38)$$

The two-pion exchange isovector tensor potential reads explicitly,

$$\begin{aligned} \widetilde{W}_T^{(2\pi)}(r) = & \frac{g_A^2}{48\pi^2 f_\pi^4} \frac{e^{-2x}}{r^6} \left\{ - \left( c_4 + \frac{1}{4M} \right) (1+x)(3+3x+x^2) \right. \\ & \left. + \frac{g_A^2}{32M} (36 + 72x + 52x^2 + 17x^3 + 2x^4) \right\} . \end{aligned} \quad (39)$$

Since  $c_4 > 0$  it is attractive and therefore cuts down the repulsive isovector tensor potential due to one-pion exchange

$$\widetilde{W}_T^{(1\pi)}(r) = \frac{g_{\pi N}^2}{48\pi M^2} \frac{e^{-x}}{r^3} (3 + 3x + x^2) . \quad (40)$$

At a distance  $r = 1/m_\pi = 1.43$  fm the two-pion exchange isovector tensor potential is  $-22.5\%$  of the one-pion exchange isovector tensor potential. Such a reduction is indeed required by phenomenology [1]. In Fig.9 we show the reduced isovector tensor potentials  $(m_\pi r)^3 \widetilde{W}_T(r)$  for distances  $1 \text{ fm} < r < 4 \text{ fm}$ . Note that already at  $r = 2.5$  fm the two-pion exchange effects start to become visible. The  $1/M$ -terms in eq.(39) are very small.

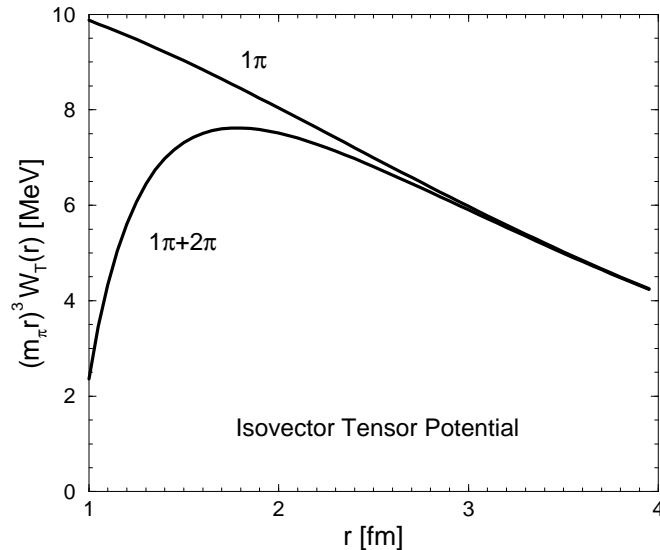


Fig.9: The reduced isovector tensor potentials  $(m_\pi r)^3 \widetilde{W}_T(r)$  in  $r$ -space.

Furthermore, we give the two-pion exchange isoscalar tensor and isovector central potentials in coordinate space. Using  $\text{Im} L(-i\mu) = -(\pi/2\mu)\sqrt{\mu^2 - 4m_\pi^2}$  for the relevant

loop function, one finds after some calculation that these can be expressed in terms of two modified Bessel-functions,

$$\begin{aligned} \tilde{V}_T(r) = & \frac{g_A^4 m_\pi}{128\pi^3 f_\pi^4 r^4} \left\{ -12x K_0(2x) - (15 + 4x^2) K_1(2x) \right. \\ & \left. + \frac{3\pi e^{-2x}}{8Mr} (12x^{-1} + 24 + 20x + 9x^2 + 2x^3) \right\}, \end{aligned} \quad (41)$$

$$\begin{aligned} \tilde{W}_C(r) = & \frac{m_\pi}{128\pi^3 f_\pi^4 r^4} \left\{ [1 + 2g_A^2(5 + 2x^2) - g_A^4(23 + 12x^2)] K_1(2x) \right. \\ & + x[1 + 10g_A^2 - g_A^4(23 + 4x^2)] K_0(2x) + \frac{g_A^2 \pi e^{-2x}}{4Mr} [2(3g_A^2 - 2) \\ & \left. \cdot (6x^{-1} + 12 + 10x + 4x^2 + x^3) + g_A^2 x(2 + 4x + 2x^2 + 3x^3)] \right\}. \end{aligned} \quad (42)$$

The asymptotic behaviour for large distances  $r$  is  $e^{-2m_\pi r}/r^{5/2}$  for  $\tilde{V}_T(r)$  and  $e^{-2m_\pi r}/r^{3/2}$  for  $\tilde{W}_C(r)$ , neglecting the  $1/M$ -terms. This long range behaviour is determined by the box graphs (proportional to  $g_A^4$ ). In the chiral limit  $m_\pi = 0$  both display a  $1/r^5$  powerlike fall-off. Since the modified Bessel-functions  $K_{0,1}(2m_\pi r)$  are positive and  $g_A > 1$  one sees that  $\tilde{V}_T(r)$  and  $\tilde{W}_C(r)$  are both negative throughout. The finite range part of the two-pion exchange isovector central potential is attractive and not repulsive as one would expect from analogies with the  $\rho$ -meson. It is very interesting to see how this unexpected attraction comes about. In the bubble and triangle diagrams (proportional to  $g_A^0$  and  $g_A^2$ ) of Fig.2 a two-pion state with the quantum numbers of the  $\rho$ -meson is emitted from one nucleon. As can be seen from the explicit expression in eq.(42) these processes indeed lead to an isovector central repulsion. However, the box diagrams (proportional to  $g_A^4$ ) are much more attractive and overcompensate the expected isovector central repulsion. The isovector central and isoscalar tensor potentials are shown in Fig.10. We remark that for these the  $1/M$ -terms are not negligible.

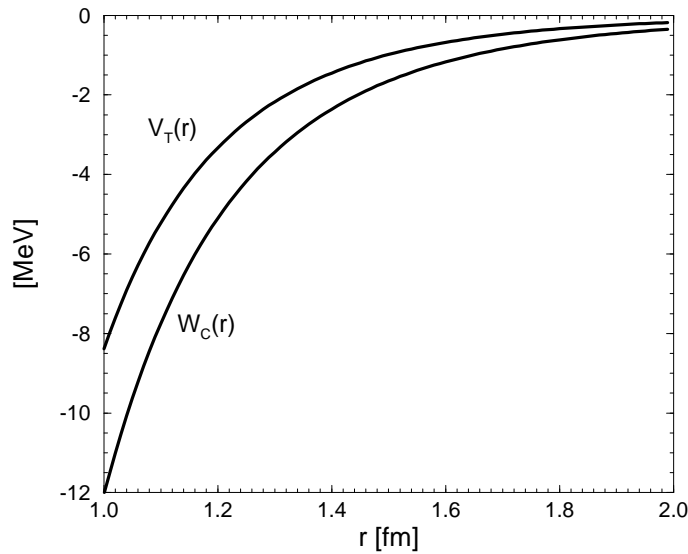


Fig.10: The isovector central potential  $\tilde{W}_C(r)$  and the isoscalar tensor potential  $\tilde{V}_T(r)$  generated by irreducible chiral two-pion exchange in  $r$ -space.

At  $r = 1$  fm they lead to an almost 50% reduction of the leading term, while at larger distances this reduction gets smaller.

Two-pion exchange spin-spin potentials in coordinate space (accompanying the operator  $\vec{\sigma}_1 \cdot \vec{\sigma}_2$ ) have an analogous spectral representation

$$\tilde{V}_S(r) = -\frac{1}{3\pi^2 r} \int_{2m_\pi}^{\infty} d\mu \mu^3 e^{-\mu r} \text{Im } V_T(-i\mu) . \quad (43)$$

We find from the chiral two-pion exchange the following isoscalar and isovector spin-spin potentials,

$$\tilde{V}_S(r) = \frac{g_A^4 m_\pi}{32\pi^3 f_\pi^4 r^4} \left\{ 3x K_0(2x) + (3 + 2x^2) K_1(2x) - \frac{3\pi e^{-2x}}{16Mr} (6x^{-1} + 12 + 11x + 6x^2 + 2x^3) \right\} , \quad (44)$$

$$\tilde{W}_S^{(2\pi)}(r) = \frac{g_A^2}{48\pi^2 f_\pi^4} \frac{e^{-2x}}{r^6} \left\{ \left( c_4 + \frac{1}{4M} \right) (1+x)(3+3x+2x^2) - \frac{g_A^2}{16M} (18 + 36x + 31x^2 + 14x^3 + 2x^4) \right\} . \quad (45)$$

Both are positive and thus add to the one-pion exchange spin-spin potential

$$\tilde{W}_S^{(1\pi)}(r) = \frac{g_{\pi N}^2 m_\pi^2}{48\pi M^2} \frac{e^{-x}}{r} . \quad (46)$$

In Fig.11 the spin-spin potentials due to one-pion-exchange (isovector) and two-pion exchange (isoscalar and isovector) are shown for  $1 \text{ fm} < r < 2 \text{ fm}$ . The isoscalar spin-spin potential is again reduced appreciably by the  $1/M$ -terms in eq.(44). We also note that the terms proportional to  $g_A^4$  involving the modified Bessel-functions  $K_{0,1}(2x)$  in eqs.(41,42,44) agree with the earlier calculation of ref. [25].

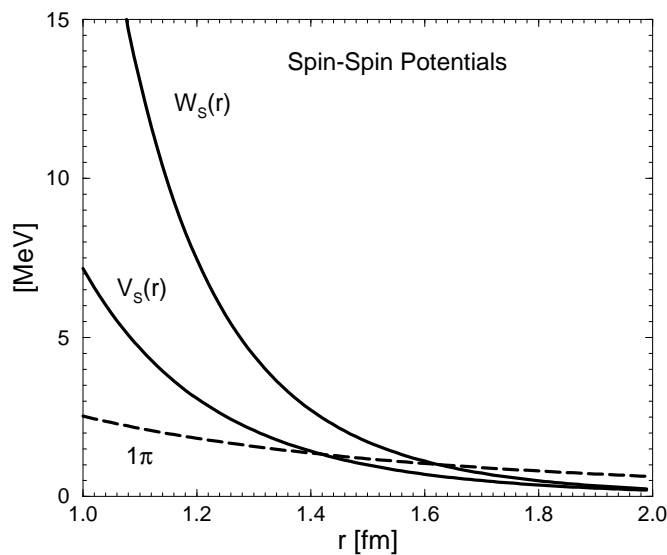


Fig.11: Spin-spin NN-potentials due to one-pion exchange (dashed line) and two-pion exchange (full lines) in  $r$ -space.



Spin-orbit potentials in coordinate space (accompanying the standard spin-orbit operator  $-\frac{i}{2}(\vec{\sigma}_1 + \vec{\sigma}_2) \cdot (\vec{r} \times \vec{\nabla}_r)$ ) have a spectral representation,

$$\tilde{V}_{SO}(r) = \frac{1}{\pi^2 r^3} \int_{2m_\pi}^{\infty} d\mu \mu (1 + \mu r) e^{-\mu r} \text{Im} V_{SO}(-i\mu) . \quad (47)$$

We find from chiral two-pion exchange the following isoscalar and isovector spin-orbit potentials,

$$\tilde{V}_{SO}(r) = -\frac{3g_A^4}{64\pi^2 M f_\pi^4} \frac{e^{-2x}}{r^6} (1+x)(2+2x+x^2) , \quad (48)$$

$$\tilde{W}_{SO}(r) = \frac{g_A^2(g_A^2 - 1)}{32\pi^2 M f_\pi^4} \frac{e^{-2x}}{r^6} (1+x)^2 . \quad (49)$$

At  $r = 1/m_\pi = 1.43$  fm these finite range two-pion exchange spin-orbit potentials are  $\tilde{V}_{SO}(1/m_\pi) = -1.97$  MeV and  $\tilde{W}_{SO}(1/m_\pi) = 0.22$  MeV. The isovector spin-orbit potential  $\tilde{W}_{SO}(r)$  is very small and repulsive. However, the isoscalar spin-orbit potential  $\tilde{V}_{SO}(r)$  from irreducible two-pion exchange is quite large and attractive and it turns out to be in very good agreement with the sum of the phenomenological  $\sigma(550)$ - and  $\omega(782)$ -exchange contributions. In Fig.12, these spin-orbit potentials are shown for distances  $1 \text{ fm} < r < 2$  fm. Finally, we note that the expressions for the two-pion exchange spin-orbit potentials eq.(48,49) agree with the earlier calculation of ref. [26]. Actually, we agree on all terms with earlier calculations, except those proportional to  $g_A^4/M$  coming from the planar box graph and contributing to the central, spin-spin and tensor potentials. This type of relativistic correction is only well defined if the relativistic correction to the iterated one-pion exchange is specified (as done here in eq.(24)).

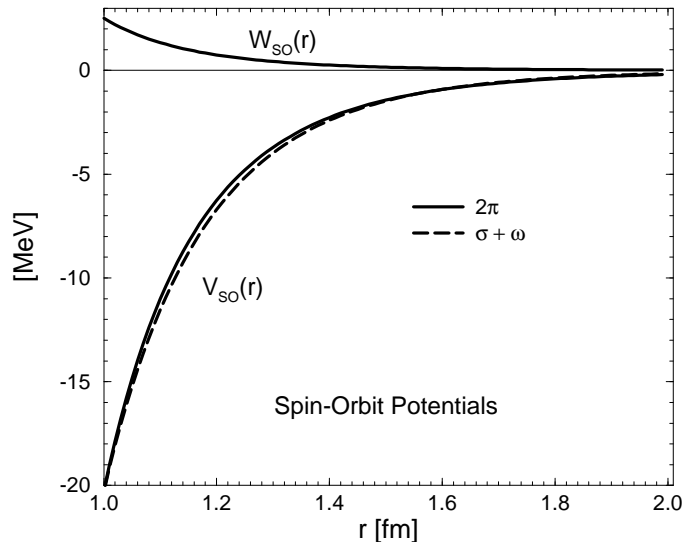


Fig.12: Isoscalar and isovector spin-orbit NN-potentials of two-pion exchange in  $r$ -space (full curves). The dashed line shows the isoscalar spin-orbit potential from  $\sigma$ - and  $\omega$ -exchange [1,5].

As a summary we find, that all irreducible two-pion exchange NN-potentials are of van-der-Waals type. They show an asymptotic exponential behaviour,  $e^{-2m_\pi r}/r^n$ ,  $n =$

$\frac{3}{2}, 2, \frac{5}{2}, 3, 4$ , with a decay length  $(2m_\pi)^{-1} \simeq 0.7$  fm. Near the origin  $r = 0$  they become singular as  $r^{-5}$  or  $r^{-6}$ . The strongly attractive parts of the potentials  $V_C$ ,  $W_S$  and  $W_T$  below  $r = 1.5$  fm are responsible for the overestimate of the D-wave phase shifts and  $\epsilon_2$  in Fig.3. Wave-functions of D-states still probe to an appreciable amount the NN-potentials below  $r = 1.5$  fm, which in our calculation come out too strong in most cases. In order to improve the D-wave observables one has to add either repulsive zero-range counter terms or an explicit  $\omega(782)$ -meson.

Finally, we have to spell out a warning in order to avoid confusion. The coordinate space potentials calculated here and the momentum space functions of section IIB are not related through each other by ordinary Fourier- and inverse Fourier-transformation. Both of them are too singular at  $r = 0$  or  $q \rightarrow \infty$  that these transforms would exist. The polynomial pieces  $(\alpha + \beta q^2)$  of the momentum space functions generate potentials proportional to zero-range delta-functions and Laplacians of delta-functions with divergent constants. On the other hand the Fourier-transform of a potential as singular as  $r^{-5}$  or  $r^{-6}$  near the origin has a divergent polynomial piece in it. Only in a loose sense, i.e. modulo zero-range  $\delta^3(\vec{r})$ -terms and linear polynomials in  $q^2$ , are the coordinate space potentials (presented in this section) and the momentum space functions of irreducible two-pion exchange (section IIB) related by Fourier-transformation. For the observables we have considered in this work, the phase shifts with  $L \geq 2$  and mixing angles with  $J \geq 2$ , these polynomial pieces and delta-function terms do not play a role at all, as we have mentioned repeatedly.

## VII. COMPARISON WITH ONE-BOSON-EXCHANGE

A detailed comparison between one-boson exchange and (irreducible) chiral two-pion exchange in momentum space is not really meaningful because of the different dependences on the momentum transfer  $q$ . Nevertheless, we find it instructive to compare at least the overall strengths of both, i.e. the values at  $q = 0$ , denoted by an overbar. These values at  $q = 0$  include also zero-range effects generated by irreducible chiral two-pion exchange.

For the isoscalar central part one finds from irreducible chiral two-pion exchange and  $\sigma + \omega$ -exchange at  $q = 0$ ,

$$\begin{aligned} \overline{V}_C^{(2\pi)} &= \frac{15g_A^2 m_\pi^3}{16\pi f_\pi^4} \left( \frac{6}{5}c_1 - c_3 - \frac{g_A^2}{64M} \right) = 79 \text{ GeV}^{-2}, \\ \overline{V}_C^{(\sigma)} + \overline{V}_C^{(\omega)} &= \frac{g_\sigma^2}{M_\sigma^2} - \frac{g_\omega^2}{M_\omega^2} = (295 - 217) \text{ GeV}^{-2} = 78 \text{ GeV}^{-2}, \end{aligned} \quad (50)$$

using  $g_\sigma^2/4\pi = 7.1$  and  $g_\omega^2/4\pi = 10.6$  [1,5]. The isoscalar central attraction produced by chiral two-pion exchange is stunningly close to the sum of the individually large phenomenological  $\sigma$ -attraction and  $\omega$ -repulsion. Note that the isoscalar central attraction due two-pion exchange is a chiral symmetry breaking effect  $\sim m_\pi^3$ . The following interpretation of the numerical result, eq.(50), is tempting. In the chiral limit the phenomenological  $\sigma$ -attraction and  $\omega$ -repulsion will cancel each other entirely. On the other hand, it has been shown recently [22] that in this case,  $V_C^{(\sigma)}(r) + V_C^{(\omega)}(r) \simeq 0$ , the so-called pseudospin symmetry observed in nuclear shell model spectra, can be explained very naturally. This suggests a strong connection between chiral symmetry of QCD and pseudo-spin symmetry in nuclei. Of course, more detailed and quantitative work is necessary to put this conjecture on a firm basis.

We have also compared irreducible chiral two-pion exchange with OBE in other channels. No clear relation between OBE ( $\sigma, \rho, \omega$ ) and chiral two-pion exchange can be deduced from this comparison. The physics behind both is also rather different. Whereas the OBE parametrizes effects of (strongly) correlated and resonant multi-pion exchange, the chiral two-pion exchange (to one-loop) involves only soft pions without self-interaction.

### VIII. SUMMARY

In this work we have gone one step further in a model independent description of the low-energy NN-interaction. In addition to the one-pion exchange, which is known to dominate the high angular momentum partial waves, we have included two-pion exchange processes based on the most general chiral effective Lagrangian. We have performed a one-loop calculation of the NN T-matrix using covariant perturbation theory and dimensional regularization throughout. We solved the so-called pinch singularity problem occurring in the planar box diagram by subtracting the iterated one-pion exchange proportional the nucleon mass  $M$ . In fact we calculated here all one-loop contributions to the NN T-matrix at second and third order in the small momentum expansion.

No pion-nucleon form factor is generated to modify the point-like one-pion exchange. Restricting ourselves to peripheral NN-phases (phase shifts with orbital angular momentum  $L \geq 2$  and mixing angles with  $J \geq 2$ ) the calculation does not involve a single adjustable parameter. This feature allows for a clean test of chiral symmetry in the two-nucleon system. Comparing to existing NN phase shift analyses we find partial agreement in the D-waves up to  $T_{lab} = 150$  MeV but also appreciable deviations. In particular, we find that the isoscalar central attraction generated by chiral two-pion exchange is far too strong for distances  $1 \text{ fm} < r < 2 \text{ fm}$ . This points towards the importance of shorter range effects in the D-waves.

Increasing the orbital angular momentum  $L$  the agreement between the chiral prediction and the data improves gradually also for larger energies up to the  $NN\pi^0$ -threshold,  $T_{lab} = 280$  MeV. There is indeed a kinematical window where chiral symmetry governs the nucleon-nucleon interaction. Examples for this are the mixing angle  $\epsilon_3$  and the  $^1G_4$  and  $^3G_5$  phase shifts, where the chiral corrections close the sizeable gaps between the one-pion exchange approximation and the data. In the high angular momentum partial waves ( $L \geq 5$ ) we find a faster convergence to the one-pion exchange as obtained in the empirical NN phase shift analyses.

The calculation presented here incorporates via one- and two-pion exchange the long and medium long range components of the NN-interaction in a model independent way. Therefore we propose the chiral NN phase shifts with  $L \geq 3$  and mixing angles with  $J \geq 3$  to be used as input in a future NN phase shift analysis. This way one could find out whether the small differences to existing phase shift analyses are significant in a direct comparison with NN-scattering data, namely angular distributions of differential cross sections and polarization observables.

We have given explicit expressions for the isoscalar/isovector central, spin-spin, tensor and spin-orbit potentials in coordinate space generated by irreducible chiral two-pion exchange. They are of van-der-Waals type with an exponential asymptotic behaviour,  $e^{-2m_\pi r}/r^n$ . The isoscalar central potential is about twice as attractive as the one of the  $\sigma(550)$ -boson in the Bonn potential. Contrary to expectations the two-pion isovector

central potential is attractive, because the contribution of the box graphs is numerically dominant.

The one-pion isovector tensor potential is reduced by the two-pion exchange contribution. The sum of both is in agreement with the phenomenological Paris potential above  $r = 1.2$  fm. The two-pion exchange isoscalar spin-orbit potential is surprisingly close to the sum of the phenomenological  $\sigma(550)$ - and  $\omega(782)$ -exchange contributions.

It is needless to say, that the chiral approach to NN-interaction presented here can (at the moment) not substitute for the successful phenomenological models as a whole. In nuclear physics applications the low partial waves (S, P, D) are the more relevant ones and chiral symmetry may be of minor importance for these. A combination of chiral dynamics together with short range contributions e.g. from  $\omega$ -exchange might help and will be explored further.

### Acknowledgment

We thank A. Jackson, M. Lutz and R. Machleidt for useful discussions.

### APPENDIX: ANTI-SYMMETRIZED NN T-MATRIX

Even though the (direct) NN T-matrix of the form eq.(4) is sufficient to calculate all observables it has one deficit. It does not incorporate the Pauli exclusion principle and therefore it has non-vanishing matrix elements in the Pauli-forbidden NN-states with even  $I + S + L$ . This deficit is cured by subtracting the T-matrix which results from the exchange of the two out-going nucleon lines,

$$\mathcal{T}_{NN} - \mathcal{A}[\mathcal{T}_{NN}]. \quad (51)$$

The exchange operation  $\mathcal{A}$  involves a left-multiplication with the isospin exchange operator  $(1 + \vec{\tau}_1 \cdot \vec{\tau}_2)/2$ , a left-multiplication with the spin exchange operator  $(1 + \vec{\sigma}_1 \cdot \vec{\sigma}_2)/2$  and a substitution  $\vec{p}' \rightarrow -\vec{p}'$  and  $z \rightarrow -z$  in the scalar functions  $V_C(p, z), \dots, W_Q(p, z)$ . Evidently, twofold application of the exchange operation  $\mathcal{A}$  is the identity operation,  $\mathcal{A} \circ \mathcal{A} = 1$ , and thus  $\mathcal{T}_{NN} - \mathcal{A}[\mathcal{T}_{NN}]$  is indeed anti-symmetric. The exchange T-matrix  $\mathcal{A}[\mathcal{T}_{NN}]$  has the same decomposition with respect to the ten isospin-spin operators as  $\mathcal{T}_{NN}$  in eq.(4), only the scalar functions  $V_C(p, z), \dots, W_Q(p, z)$  are replaced by different ones, called  $\mathcal{A}[V_C(p, z)], \dots, \mathcal{A}[W_Q(p, z)]$ . The latter have the following explicit form (suppressing the arguments  $p$  and  $z$ ),

$$\begin{aligned} \mathcal{A}[V_C] &= \frac{1}{4} \left[ V_C + 3W_C + 3V_S + 9W_S + q^2(V_T + 3W_T) + p^4(1 - z^2)(V_Q + 3W_Q) \right]_{z \rightarrow -z}, \\ \mathcal{A}[W_C] &= \frac{1}{4} \left[ V_C - W_C + 3V_S - 3W_S + q^2(V_T - W_T) + p^4(1 - z^2)(V_Q - W_Q) \right]_{z \rightarrow -z}, \\ \mathcal{A}[V_S] &= \frac{1}{4} \left[ V_C + 3W_C - V_S - 3W_S + q^2(V_T + 3W_T) + p^4(z^2 - 1)(V_Q + 3W_Q) \right]_{z \rightarrow -z}, \\ \mathcal{A}[W_S] &= \frac{1}{4} \left[ V_C - W_C - V_S + W_S + q^2(V_T - W_T) + p^4(z^2 - 1)(V_Q - W_Q) \right]_{z \rightarrow -z}, \\ \mathcal{A}[V_T] &= \frac{1}{2} \left[ \frac{z - 1}{z + 1} (V_T + 3W_T) \right]_{z \rightarrow -z}, \\ \mathcal{A}[W_T] &= \frac{1}{2} \left[ \frac{z - 1}{z + 1} (V_T - W_T) \right]_{z \rightarrow -z}, \end{aligned}$$

$$\begin{aligned}
\mathcal{A}[V_{SO}] &= \frac{1}{2} \left[ -V_{SO} - 3W_{SO} \right]_{z \rightarrow -z} , \\
\mathcal{A}[W_{SO}] &= \frac{1}{2} \left[ W_{SO} - V_{SO} \right]_{z \rightarrow -z} , \\
\mathcal{A}[V_Q] &= \frac{1}{2} \left[ V_Q + 3W_Q - \frac{2}{p^2(z+1)} (V_T + 3W_T) \right]_{z \rightarrow -z} , \\
\mathcal{A}[W_Q] &= \frac{1}{2} \left[ V_Q - W_Q - \frac{2}{p^2(z+1)} (V_T - W_T) \right]_{z \rightarrow -z} , \tag{52}
\end{aligned}$$

with the notation  $[f(p, z)]_{z \rightarrow -z} = f(p, -z)$ . The matrix elements of  $\mathcal{A}[\mathcal{T}_{NN}]$  in the LSJ-basis are readily evaluated replacing  $V_C, \dots, W_Q$  by  $\mathcal{A}[V_C], \dots, \mathcal{A}[W_Q]$  in eqs.(5-9). Making a further substitution  $z \rightarrow -z$  and using the property  $P_J(-z) = (-1)^J P_J(z)$  of the Legendre polynomials, one finds that the original matrix elements of  $\mathcal{T}_{NN}$  are reproduced up to an important sign,

$$\langle L'SJ | \mathcal{A}[\mathcal{T}_{NN}] | LSJ \rangle = (-1)^{I+S+L} \langle L'SJ | \mathcal{T}_{NN} | LSJ \rangle . \tag{53}$$

The anti-symmetrized T-matrix  $\mathcal{T}_{NN} - \mathcal{A}[\mathcal{T}_{NN}]$  has indeed the desired property, that all its matrix elements in the Pauli-forbidden NN-states (with even  $I + S + L$ ) vanish identically. Imposing the Pauli principle from the very beginning is important if one considers polynomial counter terms in order to avoid redundancy in the low-energy constants (see e.g. eq.(35) for an S-wave counter term with only two independent low-energy constants  $B, B'$ ).

## REFERENCES

- [1] T. Ericson and W. Weise, *Pions and Nuclei*, Clarendon Press, Oxford, 1988.
- [2] For a general discussion of this phenomenon see: J.R. Taylor, *Scattering Theory*, John Wiley and Sons Inc., 1972; page 245.
- [3] O. Dumbrajs et al., *Nucl. Phys.* **B216** (1983) 277.
- [4] R.A. Arndt, J.S. Hyslop and L.D. Roper, *Phys. Rev.* **D35** (1987) 121; R.A. Arndt and L.D. Roper, Scattering Analysis Interactive Dial-in Program (SAID), Virginia Polytechnic Institute and State University.
- [5] R. Machleidt, K. Holinde and Ch. Elster, *Physics Reports* **149** (1987) 1 and references therein.
- [6] G.E. Brown and A.D. Jackson, *The Nucleon-Nucleon Interaction*, North-Holland, Amsterdam, 1976; A.D. Jackson, D.O. Riska and B. Verwest, *Nucl. Phys.* **A249** (1975) 397; J.W. Durso, M. Saarela, G.E. Brown and A.D. Jackson *Nucl. Phys.* **A278** (1977) 445; M. Lacombe, B. Loiseau, J.M. Richard, R. Vinh Mau, T. Cote et al., *Phys. Rev.* **C21** (1980) 861.
- [7] S. Weinberg, *Phys. Lett.* **B251** (1990) 288; *Nucl. Phys.* **B363** (1991) 3.
- [8] C. Ordóñez, L. Ray, and U. van Kolck. *Phys. Rev. Lett.* **72** (1994) 1982; *Phys. Rev.* **C53** (1996) 2086.
- [9] V. de Alfaro, S. Fubini, G. Furlan and C. Rossetti, *Current in Hadron Physics*, North-Holland, Amsterdam, 1973 and references therein.
- [10] V. Bernard, N. Kaiser and Ulf-G. Meißner, *Nucl. Phys.* **A615** (1997) 483; *Phys. Rev.* **C52** (1995) 2185.
- [11] E. Jenkins and A.V. Manohar, *Phys. Lett.* **B255** (1991) 588; G. Ecker, *Phys. Lett.* **B336** (1994) 508.
- [12] V. Bernard, N. Kaiser and Ulf-G. Meißner, *Int. J. Mod. Phys.* **E4** (1995) 193.
- [13] G. Höhler, in Landolt-Börnstein, Vol.92b. ed. H. Schopper, Springer, Berlin, 1983.
- [14] K. Erkelenz, R. Alzetta and K. Holinde. *Nucl. Phys.* **A176** (1971) 413.
- [15] H.P. Stapp, T.L. Ypsilantis and N. Metropolis, *Phys. Rev.* **105** (1957) 302.
- [16] For the perturbative definition of the  $\pi\pi$  phase shift see: J. Gasser and Ulf-G. Meißner, *Phys. Lett.* **B258** (1991) 219.
- [17] M. Ericson and A. Figureau *J. Phys.* **G7** (1989) 1197.
- [18] J. Gasser and H. Leutwyler, *Ann. Phys. (NY)* **158** (1984) 142.
- [19] G. Ecker and M. Mojziz, *Phys. Lett.* **B335** (1996) 312.
- [20] V. Bernard, N. Kaiser, J. Kambor and Ulf-G. Meißner, *Nucl. Phys.* **B388** (1992) 315.
- [21] V.G.J. Stoks, R.A.M. Klomp, M.C.M. Rentmester and J.J. de Swart, *Phys. Rev.* **C48** (1993) 792.
- [22] J.N. Ginocchio, *Phys. Rev. Lett.* **78** (1997) 436.
- [23] M.R. Robilotta and C.A. da Rocha, *Nucl. Phys.* **A615** (1997) 391.
- [24] R. Tarrach and M. Ericson, *Nucl. Phys.* **A294** (1978) 417.
- [25] M. Taketani, S. Machida and S. Ohnuma, *Prog. Theor. Phys.* **7** (1952) 45; K.A. Brueckner and K.M. Watson, *Phys. Rev.* **92** (1953) 1023.
- [26] M. Sugawara and S. Okubo, *Phys. Rev.* **117** (1960) 605, 611.